

**Arbeit zur Erlangung des akademischen Grades
Master of Science**

**Simulation of rare processes and
electromagnetic shower components
within the Monte Carlo propagation
library PROPOSAL**

Jean-Marco Alameddine
geboren in Iserlohn

2020

Lehrstuhl für Experimentelle Physik V
Fakultät Physik
Technische Universität Dortmund

Erstgutachter: Prof. Dr. Dr. Wolfgang Rhode
Zweitgutachter: Prof. Dr. Kevin Kröninger
Abgabedatum: 14. Februar 2020

Abstract

PROPOSAL is a C++ Monte Carlo simulation library used to describe the propagation of highly energetic particles. These particles can, for example, be induced by atmospheric air showers or produced from interactions of astrophysical high-energy neutrinos with matter, observed with experiments such as the IceCube Neutrino Observatory. In this thesis, both the implementation of photon propagation as well as a more precise description of electron and positron propagation in PROPOSAL are presented. This allows PROPOSAL to be used as a propagator for the simulation of electromagnetic shower components, for example in the upcoming eighth version of the extensive air shower simulation software CORSIKA. Furthermore, rare interactions, although negligible for the average energy loss of muons but producing possibly significant detector signatures for specific analyses, are added as optional processes in PROPOSAL.

Kurzfassung

PROPOSAL ist eine C++ Monte Carlo Simulationsbibliothek zur Propagation hochenergetischer Teilchen. Diese Teilchen entstehen beispielsweise in Luftschauren oder durch die Wechselwirkung hochenergetischer, astrophysikalischer Neutrinos mit Materie. Experimente wie das IceCube Neutrino Observatory sind in der Lage Teilchen dieser Art zu beobachten. In dieser Arbeit werden sowohl die Implementation der Propagation von Photonen als auch eine verbesserte Beschreibung der Propagation von Elektronen und Positronen in PROPOSAL vorgestellt. Hierdurch ist es möglich, PROPOSAL als Propagator für die Simulation elektromagnetischer Schauer, beispielsweise in der kommenden achten Version des Luftschauer-Simulationprogrammes CORSIKA, zu verwenden. Des Weiteren wird die Einbindung seltener Prozesse als zusätzliche, optionale Wechselwirkungen in PROPOSAL beschrieben. Diese Prozesse sind zwar vernachlässigbar für den durchschnittlichen Energieverlust von Myonen in Materie, können gleichzeitig jedoch für einzelne Analysen relevante Detektorsignaturen verursachen.

Contents

1	Introduction	1
2	Large scale Monte Carlo simulation software	3
2.1	The lepton propagator PROPOSAL	3
2.1.1	Calculation of energy losses	4
2.1.2	Propagation algorithm	7
2.1.3	Muon propagation with PROPOSAL	11
2.2	The shower simulation program CORSIKA	16
2.2.1	Description of CORSIKA 7	16
2.2.2	Development of CORSIKA 8	17
2.2.3	The EGS4 computer code system	18
2.2.4	Usage of EGS4 in CORSIKA	18
3	Integration of rare processes	20
3.1	Muon pair production	20
3.1.1	Theoretical description	20
3.1.2	Implementation in PROPOSAL	22
3.1.3	Significant detector signatures	25
3.2	Weak interaction of charged leptons	28
3.2.1	Theory and data description	28
3.2.2	Implementation in PROPOSAL	29
3.2.3	Significant detector signatures	31
4	Propagation of electromagnetic showers	33
4.1	Electron and positron propagation in PROPOSAL	33
4.1.1	Ionization	34
4.1.2	Bremsstrahlung	38
4.1.3	Electron-positron annihilation	42
4.2	Photon propagation in PROPOSAL	46
4.2.1	Pair production by photons	46
4.2.2	Compton scattering	50
4.3	Electromagnetic shower propagation with PROPOSAL	53

5 Conclusion and outlook	58
5.1 Conclusion	58
5.2 Outlook	59
A Atomic form factors for photo pair production	60
A.1 Hydrogen and Helium	60
A.2 Lithium and Beryllium	61
A.3 Heavier elements	62
B Constants and variables	64
C Reproducibility	65
Bibliography	66

1 Introduction

The field of astroparticle physics deals with the study of highly energetic charged particles, gamma-rays or neutrinos of extraterrestrial origin. Information obtained from analyzing these messenger particles can provide insights into astrophysical sources, answer cosmological questions or improve the understanding of elementary particle physics. One important experimental facility is the IceCube Neutrino Observatory, a large scale particle detector located at the geographical South Pole searching for high energy neutrinos [2].

To be able to analyze obtained experimental data, software providing adequate Monte Carlo simulations, i.e. simulations with both sufficient quantity and quality, is required. The lepton propagator PROPOSAL, the main focus of this work, is a Monte Carlo simulation library describing interactions of highly energetic leptons in media. The main application of PROPOSAL is the simulation of energy losses of muon and tau leptons in ice within the simulation chain of IceCube, however, PROPOSAL is publicly available and may be used as a standalone library. In this work, extensions with emphasis on two different aspects of PROPOSAL are presented.

The first focus lays on the description of rare processes, namely the production of muon pairs and the conversion of a charged lepton to a neutrino under the exchange of a W boson. Both processes are, although highly suppressed and therefore negligible for the average energy loss of muons, producing significant detector signatures, for example in the IceCube detector. To provide a tool for analyses regarding these signatures, both interactions are implemented as optional, additional processes in PROPOSAL.

While PROPOSAL has originally been optimized for muon and tau propagation, the underlying modular code structure can be used to propagate particles of any type. As a second focus of this thesis, both photon propagation and a more precise description of electron and positron propagation in PROPOSAL are realized by implementing new processes as well as by adding new, optimized parametrizations of existing processes. Being able to propagate electrons, positrons and photons accurately, PROPOSAL can be used to propagate all particles in an electromagnetic shower. This allows the air shower simulation program CORSIKA to simulate a full

1 Introduction

air shower using PROPOSAL as an electromagnetic model in its upcoming eighth version that is currently in development.

This thesis is structured as follows. A general description of the large scale Monte Carlo simulation software packages PROPOSAL and CORSIKA is given in section 2. The implementation of the rare processes muon pair production and the weak interaction of charged leptons in PROPOSAL is described in section 3. An overview of analyses where these processes may portray a significant contribution is given as well. Section 4 explains the implementation of a correct description of electron, positron and photon propagation in PROPOSAL. Furthermore, as a proof of concept for an implementation of PROPOSAL as an electromagnetic model in CORSIKA 8, the results of a Python script simulating simple electromagnetic showers using PROPOSAL are presented.

2 Large scale Monte Carlo simulation software

Modern physical experiments often produce extremely large quantities of data. In order to obtain physical results, these datasets need to be evaluated. Here, using computational methods of multivariate analyses is often inevitable due to the complexity and multiplicity of the data.

One important task that needs to be performed is the signal-background separation to reject events that are irrelevant for the conducted analysis. Examples are the gamma-hadron separation in high-energy gamma-ray astronomy [37] or the separation of atmospheric muons from neutrino-induced muons in the IceCube Neutrino Observatory [5]. Signatures from signal and background events are separated by classifiers, deciding whether an event is labeled as signal or background, for example by random forests. To be able to use a classifier on a given dataset, the underlying model needs to be trained first using data from Monte Carlo simulations where it is known whether the generated signature belongs to a signal or a background event. When generating Monte Carlo simulations, both high quality and quantity of simulation data are important and need to be taken into account when writing a simulation program.

Two examples of Monte Carlo simulation software packages, the lepton propagator PROPOSAL and the air shower simulation program CORSIKA, are presented in the following section. A common characteristic of both programs is that particles traversing large distances need to be simulated both correctly and efficiently, requiring a trade-off between accuracy and computation time.

2.1 The lepton propagator PROPOSAL

PROPOSAL (**P**ropagator with **O**ptimal **P**recision and **O**ptimized **S**peed for **A**ll **L**eptons) is a Monte Carlo simulation library capable of simulating the interactions of high energy leptons. The original program called MMC (**M**uon **M**onte **C**arlo) has been written in the programming language Java focusing on a precise but also fast muon and tau propagation [10]. On this basis, MMC has been rewritten within a dissertation to create the C++ library PROPOSAL [32]. Additionally, PROPOSAL can now be used in the programming language Python through a wrapper. More

modern programming concepts such as polymorphism and a modular code structure were introduced in a recent update of PROPOSAL [15].

The current version of the code is publicly available on GitHub¹ and can be used under the terms of a modified LGPL license. Examples of applications are the neutrino observatories IceCube and RNO who use PROPOSAL as a part of their simulation chain [30].

2.1.1 Calculation of energy losses

Energy losses of particles form the basis for the propagation algorithm in PROPOSAL. Assuming a particle with an initial energy E_i , an energy loss is described by its absolute value

$$\nu = E_i \cdot v \quad (2.1)$$

where v describes the relative energy loss of the particle and $E_f = E_i - \nu$ the final particle energy. Processes causing energy losses and implemented are

- bremsstrahlung [28],
- ionization [41, 44],
- photonuclear interactions [4, 9] and
- pair production of an electron-positron pair [27, 33]

with references to descriptions of the default parametrizations used in PROPOSAL. Alternative parametrizations, for example recently improved bremsstrahlung and pair production cross sections provided by [43], are available as well and can be used optionally.

Quantitatively, the interaction probability for a process is described by its cross section σ . To describe the interaction probability with respect to a specific variable in the final state, the cross section can be written in a differential form, for example $d\sigma/dv$.

In principle, this information could be used right away to sample energy losses from differential cross sections, which are treated as probability density functions, by using inverse sampling. However, this approach would cause two immediate problems: Firstly, the propagation process would be very time-inefficient since small energy losses, especially below the energy threshold of a detector, would be sampled individually. Secondly, numerical problems will occur due to the nature of the bremsstrahlung interaction: Since photons are massless, the bremsstrahlung cross

¹<https://github.com/tudo-astroparticlephysics/PROPOSAL>

section diverges for $v \rightarrow 0$, making inverse sampling over the whole parameter range impossible.

As a solution, PROPOSAL differentiates between continuous and stochastic energy losses. The energy cut parameter v'_{cut} is defined as

$$v'_{\text{cut}} = \min [e_{\text{cut}}/E, v_{\text{cut}}] \quad (2.2)$$

with a relative energy cut v_{cut} and an absolute energy cut e_{cut} . Energy losses with $v > v'_{\text{cut}}$ are treated as stochastic losses, meaning that every interaction with a relative energy loss above the cut is treated individually. Energy losses with $v < v'_{\text{cut}}$, however, are treated as continuous losses, meaning that an averaged energy loss per distance is calculated from all energy losses below the cut and applied to the particles during propagation. Both parameters e_{cut} and v_{cut} can be set, or disabled, separately. By enabling both parameters simultaneously, the definition in (2.2) ensures that losses above an absolute detector threshold e_{cut} are treated as stochastic even if their relative value is below v_{cut} .

The propagation algorithm in PROPOSAL consists of several, consecutively executed propagation steps where each step consists of continuous losses and a stochastic loss, see section 2.1.2 for a detailed description. To perform one propagation step, it is necessary to have a mathematical expression to sample the next stochastic loss.

Let E_i be the initial energy of a particle and

$$P(E_f \leq E \leq E_i) = - \int_{E_i}^{E_f} p(E) \, dE \quad (2.3)$$

a cumulative distribution function describing the probability for a stochastic loss at a particle energy $E \geq E_f$. With inverse sampling, this function can be used to sample the remaining particle energy E_f just before the next stochastic interaction will occur.

To derive an expression for (2.3), the distance between the initial particle position x_i and the position of the stochastic loss x_f is discretized into sections of Δx . The probability for a stochastic loss after a distance of $x_f - x_i$, without any stochastic losses in the interval (x_i, x_f) , can be described as

$$\begin{aligned} \Delta P(x_f) &= P(x_f + \Delta x) - P(x_f) \\ &= (1 - \sigma(x_i)\Delta x_i) \cdot (1 - \sigma(x_{i+1})\Delta x_{i+1}) \cdot \dots \cdot (1 - \sigma(x_{f-1})\Delta x_{f-1}) \cdot \sigma(x_f)\Delta x_f \\ &\approx \exp \left(- \sum_{j=i}^{f-1} \sigma(x_j)\Delta x_j \right) \cdot \sigma(x_f)\Delta x_f \end{aligned} \quad (2.4)$$

where σ describes the probability for a stochastic loss. Note that $\Delta x \ll 1$ was used in the last step. In a differential form, this relation can be written as

$$dP(x_f) = \exp\left(-\int_{x_i}^{x_f} \sigma(x) dx\right) \cdot \sigma(x_f) dx_f. \quad (2.5)$$

To transfer the dependency on the location x to a dependency on the energy E , the relation

$$f(E) = -\frac{dE}{dx} = E \frac{N_A}{A} \int_{v_{\min}}^{v'_{\text{cut}}} v \frac{d\sigma}{dv} dv, \quad (2.6)$$

with the Avogadro constant N_A and the mass number A of the current medium², is introduced. Here, $f(E)$ describes the continuous energy losses between two stochastic losses and is calculated by taking the average energy loss for all interactions below the energy cut v'_{cut} .

Applying (2.6) on (2.5) yields

$$dP(E_f) = \exp\left(\int_{E_i}^{E_f} \frac{\sigma(E)}{f(E)} dE\right) \cdot \frac{\sigma(E_f)}{-f(E_f)} dE_f. \quad (2.7)$$

The cumulative distribution function is obtained by integrating over the probabilities in (2.7):

$$\begin{aligned} P(E_f \leq E \leq E_i) &= \int_{P(E_i)=0}^{P(E_f)} dP(E_f) \\ &= \int_{E_i}^{E_f} \exp\left(\int_{E_i}^{E'} \frac{\sigma(E)}{f(E)} dE\right) \cdot \frac{\sigma(E')}{-f(E')} dE'. \end{aligned} \quad (2.8)$$

The expression in (2.8) is simplified by using the substitution

$$u(E) = \int_{E_i}^E \frac{\sigma(E')}{f(E')} dE', \quad du = \frac{\sigma(E)}{f(E)} dE \quad (2.9)$$

where the fundamental theorem of calculus has been applied to obtain the expression for du .

²For a medium composed of different atoms, an averaged sum for A is used.

It follows that

$$\begin{aligned}
 P(E_f \leq E \leq E_i) &= - \int_{E_i}^{E_f} \exp(u(E'_f)) \, du \\
 &= [\exp(u(E'_f))]_{E_i}^{E_f} \\
 &= \exp(u(E_f)) - \underbrace{\exp(u(E_i))}_{=0} \\
 &= \exp\left(\int_{E_i}^{E_f} \frac{\sigma(E)}{-f(E)} \, dE\right).
 \end{aligned} \tag{2.10}$$

By replacing the probability P in (2.10) by a random number $\xi \in (0, 1]$ the energy integral

$$\int_{E_i}^{E_f} \frac{\sigma(E)}{-f(E)} \, dE = -\log \xi, \tag{2.11}$$

originally derived in [10], is obtained. By sampling ξ , (2.11) can be used to calculate the remaining particle energy E_f just before the next stochastic energy loss will occur.

2.1.2 Propagation algorithm

The task of the propagation algorithm of PROPOSAL is to simulate the properties of the secondary particles produced in interactions as well as the properties of the initial particle after each interaction. This includes information on the energy, position, direction and time of both the propagated particle and the secondary particles.

From a technical point of view, the structure of the propagation process in PROPOSAL is determined by the concept of a "chain of responsibility". The main parts of this chain are the *Sector* objects and a *Propagator* object.

Each *Sector* is defined by its geometry (i.e. the spatial extent of the *Sector*), its medium, its energy cut settings and other sector-specific properties. The cut settings itself differentiate between various particle positions relative to a predefined *Detector* which is a region with an increased propagation accuracy. By having sectors with varying characteristics the user has the possibility to appropriately model the simulation environment.

The *Propagator* object chooses which *Sector* is responsible for the propagation of the particle at its current position. The assigned *Sector* then propagates the particle

within its borders and returns the particle to the *Propagator* object. This process is repeated either until the propagated distance of the initial particle surpasses a preset maximal propagation distance d_{\max} or until the initial particle energy falls below a preset threshold energy e_{low} .

The following steps give a simplified overview of the propagation process within a *Sector*.

Energy of the occurrence of the next interaction

According to (2.11), the remaining particle energy E_f just before the next stochastic loss will occur is sampled using a random number ξ . If

$$\xi > \exp \left(\int_{E_i}^{e_{\text{low}}} \frac{\sigma(E)}{f(E)} dE \right), \quad (2.12)$$

the sampled energy where the next stochastic loss occurs would fall below the threshold energy e_{low} . In this case, there is no stochastic loss.

If the propagated particle is able to decay, an energy where the particle decays is sampled based on its lifetime τ . Both energy values are compared and the higher energy value, together with its interaction type (stochastic loss or decay), is used for the next step³.

Particle displacement

Given the initial energy E_i and the energy of the interaction E_f , the (straight-lined) displacement is calculated with the tracking integral

$$x_f = x_i - \int_{E_i}^{E_f} \frac{dE}{f(E)} \quad (2.13)$$

where $x_f - x_i$ denotes the propagated distance. If the calculated propagated distance would exceed the distance to the sector border d , E_f is recalculated by setting $x_f = x_i + d$ in (2.13) and solving the integral equation for E_f . In this case, no interaction will occur at E_f .

³If a decay is the next interaction, the step "Simulation of the stochastic energy loss" is replaced accordingly by a decay method.

The elapsed time is determined using the time integral

$$t_f = t_i + \int_{x_i}^{x_f} \frac{dx}{v(x)} = t_i - \int_{E_i}^{E_f} \frac{dE}{f(E)v(E)} \quad (2.14)$$

with the particle velocity $v(E)$. Alternatively, the approximation $v = c$ leading to

$$t_f = t_i + \frac{x_f - x_i}{c} \quad (2.15)$$

can be used.

Optionally, PROPOSAL can apply multiple scattering effects on the calculated displacement. This changes the position of the next stochastic loss by sampling a deflection angle as well as a new direction for the particle. Currently, three different parametrizations of multiple scattering can be used in PROPOSAL: A parametrization based on Molière's theory of multiple scattering as well as two parametrizations based on a gaussian-like approximation of the Molière theory by Highland, see [19] for a detailed description of the scattering models used in PROPOSAL.

Continuous energy losses and continuous randomization

The energy loss between E_i and E_f is treated continuously according to (2.6), meaning that the particle energy is set to $E = E_f$. However, this can cause discontinuities in the energy spectrum as shown in figure 2.1.

For a sufficiently large v_{cut} , for example $v_{\text{cut}} = 0.05$ as in figure 2.1, a peak in the final muon energy spectrum appears. This peak corresponds to all muons without any stochastic losses within the propagation distance. All of these particles have the same final energy since effectively, no random numbers were used to calculate their final energy, meaning that no fluctuations of the continuous losses are taken into account. Setting the energy cut to a significantly lower value, for example $v_{\text{cut}} = 10^{-4}$ as in figure 2.1, eliminates the peak. However, the runtime for the propagation is increased by at least an order of magnitude.

As a more time-efficient solution, the option *continuous randomization* can be enabled in PROPOSAL. This applies fluctuations on the continuous loss energies sampled from a gaussian distribution. The mean of this distribution corresponds to 0, the variance is calculated by

$$\langle \Delta(\Delta E)^2 \rangle = \int_{E_i}^{E_f} \frac{E^2}{-f(E)} \left\langle \frac{d^2 E}{dx^2} \right\rangle, \quad (2.16)$$

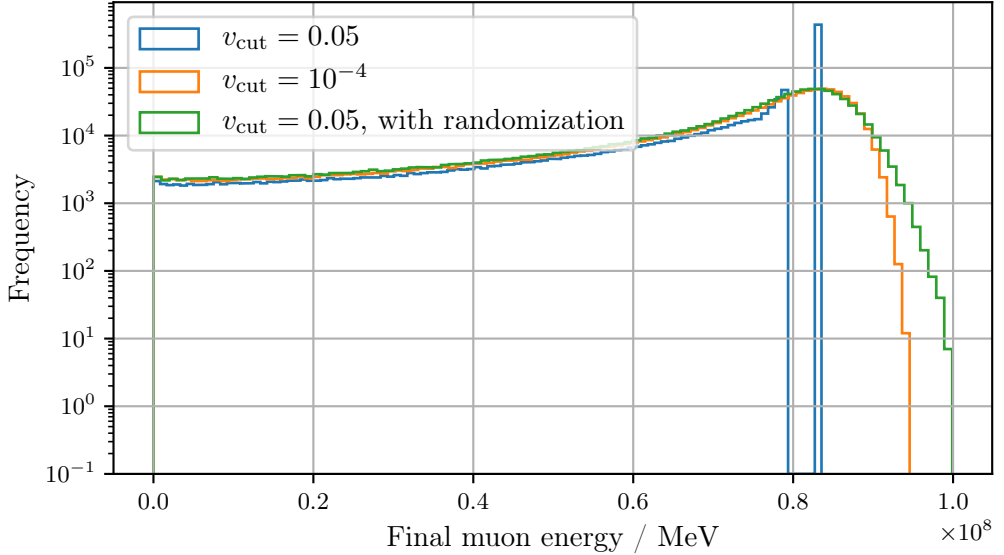


Figure 2.1: Energy spectrum of 10^6 muons with an initial energy of 10^8 MeV, propagated in 300 m of standard rock⁴. The spectrum shows the effects of an energy cut with or without continuous randomization.

where the derivation of the variance follows similar steps to the derivation of (2.11), see [10] for a detailed derivation and description. The effects can be seen in figure 2.1, the energy spectrum becomes continuous and the running time behaves similarly to the running time for the propagation without continuous randomization.

Simulation of the stochastic energy loss

If the stochastic energy loss falls inside the sector and occurs before the initial particle decays, a stochastic loss at the energy E_f is sampled. The total stochastic cross section for a process i is calculated by

$$\sigma_{\text{stoch},i}(E_f) \propto \int_{v'_{\text{cut}}}^{v_{\text{max}}} \frac{d\sigma_i(E_f)}{dv} dv. \quad (2.17)$$

Using a random number ξ_1 , the occurring process is calculated where the ratios of the process probabilities are represented by the ratios of the corresponding total

⁴Standard rock means a material with $Z = 11$, $A = 22$ and a density of $\rho = 2.65$ g/cm³, see e.g. [44] for a detailed list of material properties.

stochastic cross sections. To calculate the relative size v of the stochastic loss, the integral equation

$$\frac{1}{\sigma_{\text{stoch},i}} \int_{v'_{\text{cut}}}^v \frac{d\sigma_i}{dv} dv = \xi_2 \quad (2.18)$$

is solved for v where $\xi_2 \in [0, 1]$ is an additional random number and i the selected process.

The propagation routine is repeated by sampling the remaining particle energy before the next interaction occurs (i.e. the first step described here) until the particle has decayed, has reached the sector border or until its energy has reached the threshold energy e_{low} .

2.1.3 Muon propagation with PROPOSAL

At the end of the propagation process, PROPOSAL returns the properties of the produced secondary particles as well as the final properties of the initial particle or, if the particle decayed during propagation, its decay products. In this section the characteristic energy losses of muons are described, where ice is used exemplarily as a medium for all plots. The parametrizations for the interactions are always the default options in PROPOSAL listed in section 2.1.1. Furthermore, the Landau-Pomeranchuk-Migdal (LPM) effect for bremsstrahlung and pair production has been enabled, see [32] for a detailed description of the LPM effect.

In figure 2.2, the continuous energy losses of muons in ice, calculated according to (2.6), are shown. For this plot the energy cut has been set to $v_{\text{cut}} = v_{\text{max}}$, therefore the values shown correspond to the complete average energy losses of muons in ice. It can be seen that the average energy loss is quantitatively dominated by ionization for lower energies while e pair production, bremsstrahlung and photonuclear interactions become dominant for higher energies. Furthermore, it can clearly be seen that the parametrization

$$-\left\langle \frac{dE}{dx} \right\rangle \approx a(E) + b(E) \cdot E \quad (2.19)$$

of the average energy loss as a quasi-linear function is valid. Here, $a(E)$ corresponds to energy losses due to ionization and $b(E)$ to energy losses due to e pair production, bremsstrahlung and photonuclear interactions. The parameters $a(E), b(E)$ vary only logarithmically with energy.

Figures 2.3 and 2.4 show the stochastic losses for muons propagated in ice, the energy cuts applied here are $e_{\text{cut}} = 500 \text{ MeV}$ and $v_{\text{cut}} = 0.05$ while the muons are propagated until they decay or lost all their energy.

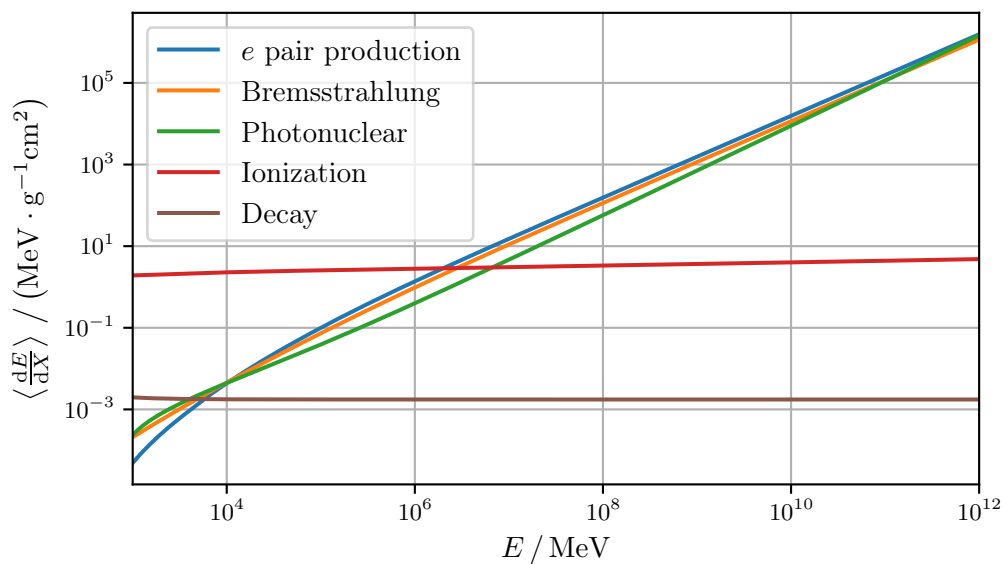


Figure 2.2: Continuous energy losses of muons in ice. No energy cuts are applied in this plot, hence this plot represents the case where all losses are treated continuously. Additionally, the average energy loss due to muon decay is shown where the muon loses, per definition, all its energy when it decays.

The histogram in figure 2.3 shows the energies of all secondary particles sorted by interaction type for $1 \cdot 10^4$ muons propagated with an initial energy of 10^8 MeV. Between about 10^3 MeV and 10^6 MeV, the energy losses are dominated by e pair production. This dominance could, for example, be used to probe the e pair production cross section in this energy range. For higher secondary energies, bremsstrahlung and photonuclear interactions are the dominant effects. Another effect that can be seen is the energy cut at $e_{\text{cut}} = 500$ MeV where the histogram cuts off abruptly. The energy losses below e_{cut} correspond to losses where $E \cdot v < e_{\text{cut}}$ but $v > v_{\text{cut}} = 0.05$. These losses are mainly ionization losses since ionization is the dominant process for low energies.

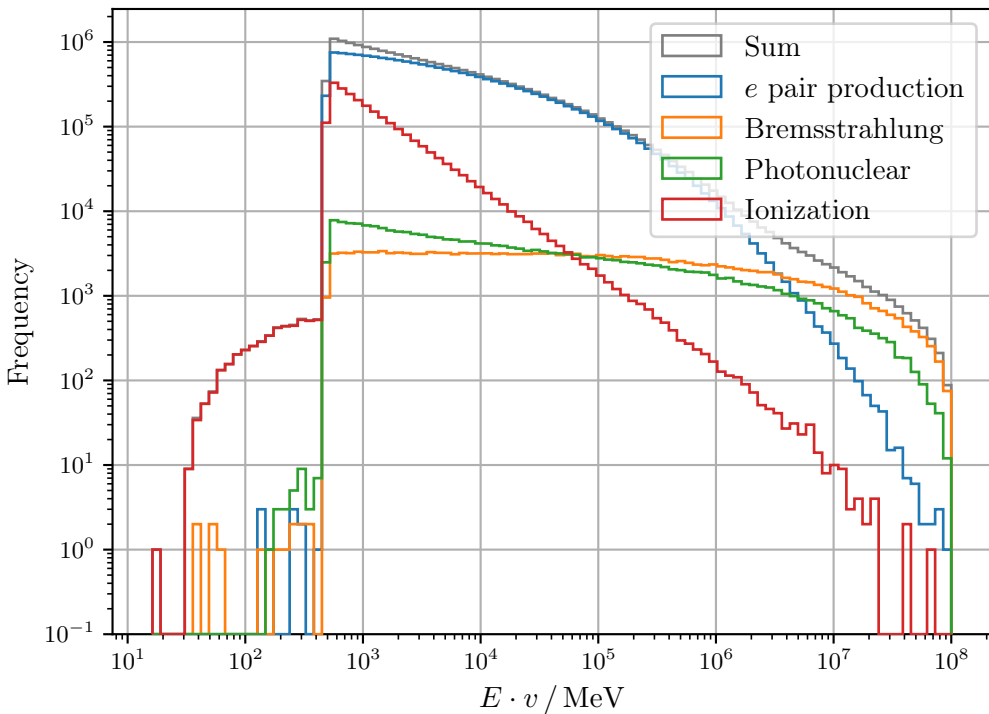


Figure 2.3: Secondary particle energy spectrum for 10^4 muons with an initial energy of 10^8 MeV, propagated in ice. The histogram shows the frequency of the stochastic losses during propagation, classified by the type of energy loss. The energy cuts applied here are $e_{\text{cut}} = 500$ MeV, $v_{\text{cut}} = 0.05$.

The two-dimensional histograms in figure 2.4 show the sorted energy losses correlated with the energy of the initial particle at the time of the interaction. Here, $5 \cdot 10^3$ muons with an initial energy of 10^{14} MeV are propagated. Table 2.1 additionally shows the sum of the secondary energy losses as well as the frequency of the energy

losses for every possible interaction.

It can be seen that bremsstrahlung and photonuclear interaction tend to have a more homogeneous spectrum where the secondary energy is less correlated with the primary energy than for ionization and pair production. For bremsstrahlung, the effects of the LPM effect can be seen since this effect causes the bremsstrahlung cross section to be suppressed for small v at very high energies. Especially for the ionization histogram, the effect of the combined e_{cut} and v_{cut} can be seen for small primary energies leading to secondary energies below e_{cut} . Table 2.1 shows that the sum of the energy losses is of the same order of magnitude for pair production, bremsstrahlung and photonuclear interaction while the contribution from ionization losses is significantly lower since the latter is mainly treated continuously. Although the energy loss contribution of pair production is comparable to bremsstrahlung and photonuclear interaction, its frequency is of several orders of magnitude higher due to its tendency to produce energy losses with smaller relative energies.

Table 2.1: Interaction-specific frequency and sum of stochastic energy losses according to figure 2.4.

Interaction	Frequency	$\sum E_{\text{prim}} \cdot v / \text{MeV}$
e pair production	1.34e+8	1.52e+17
Bremsstrahlung	3.68e+5	1.14e+17
Photonuclear	1.02e+6	2.34e+17
Ionization	3.96e+6	2.83e+10

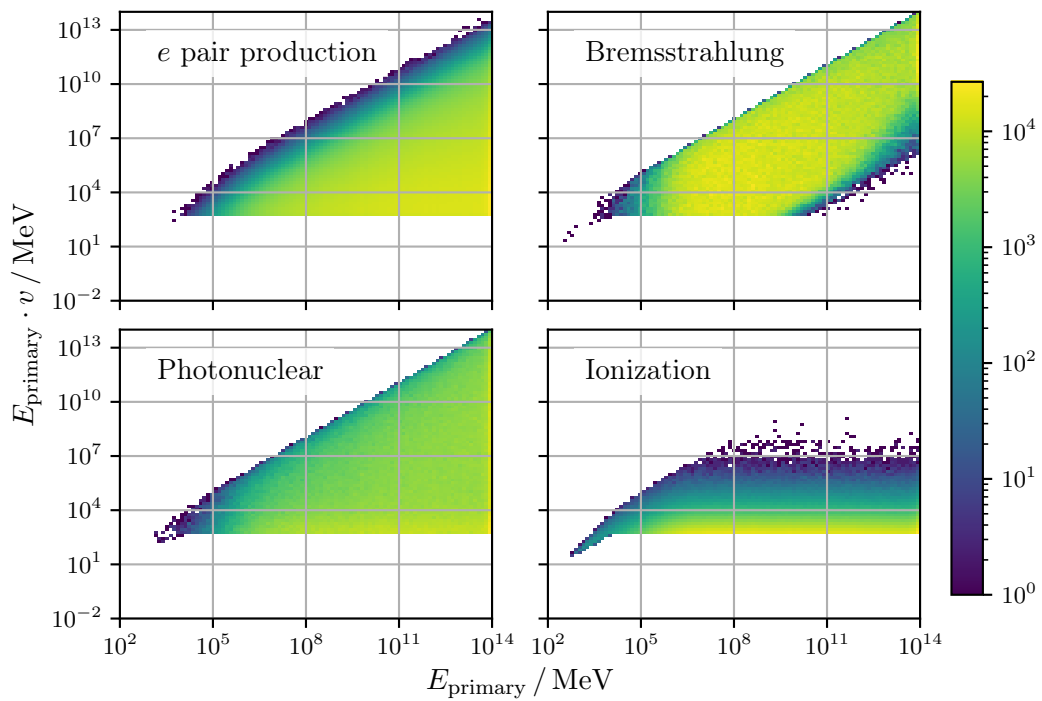


Figure 2.4: Energy spectra for $5 \cdot 10^3$ muons with an initial energy of $E = 10^{14} \text{ MeV}$ propagated in ice. For each histogram, the x-axis shows the energy of the primary particle before the stochastic loss and the y-axis the energy of the secondary particle created in the stochastic loss. The energy cuts applied here are $e_{\text{cut}} = 500 \text{ MeV}$, $v_{\text{cut}} = 0.05$.

2.2 The shower simulation program CORSIKA

CORSIKA (**C**Osmic **R**ay **S**Imulations for **K**Ascade) is a software to simulate extensive air showers induced by high-energy particles in the atmosphere. The software was originally developed to perform simulations for the extensive air shower experiment KASCADE with the first version of CORSIKA being released in October 1989 [22]. Today, CORSIKA is used as a general-purpose tool for all experiments in need of shower simulation data. At this time (February 2020), the most recent version is CORSIKA 7.7100 which has been released in October 2019.

2.2.1 Description of CORSIKA 7

CORSIKA 7 consists of routines written in the programming language FORTRAN77. It simulates interactions of electrons, positrons, photons, muons, hadrons and nuclei necessary for shower simulations with energies of up to 10^{20} eV.

As described in the CORSIKA user guide [22], the basic software structure is based on four main parts. The first three parts are responsible for the description of particle-specific physical interactions: Firstly, the transport of electrons, positrons and photons, i.e. the electromagnetic shower components, can either be described by an adapted version of the EGS4 package, a Monte Carlo software described in more detail in section 2.2.3, or analytically using NKG formulas. The description of the hadronic interactions of the shower is divided into a low-energy and a high-energy part. The former can either be described by FLUKA, by GHEISHA or by UrQMD while the latter can be described by several models including QGSJET, SIBYLL or EPOS LHC. Links to further descriptions of the individual models are provided by the CORSIKA user guide [22]. The last part of the basic structure of CORSIKA is a general program frame that is responsible for general tasks including particle tracking, particle decays or organizing dynamic particle data in a stack data structure.

The general process of shower propagation in CORSIKA can be described as follows: At first, CORSIKA samples an initial particle, inducing the air shower, from a pre-defined distribution. This particle is propagated where the treatment of the interactions depends on the interaction models chosen by the user. Further effects during the propagation step, for example deflection by a magnetic field, are applied here as well. Created secondary particles are saved temporarily on a stack. After the current particle interacted, the next particle is read from the stack and propagated as well until its energy falls below a certain threshold and the particle is removed from the simulation. Output data with information on all secondary particles on a pre-selected observation level, including particle types, locations, directions and

arrival times are generated continuously during the simulation process and can afterward be further processed by the user. As soon as the particle stack is empty, the simulation continues by sampling another primary particle initiating the next air shower.

Additional modules changing the program sequence or adding new physical properties can be loaded into CORSIKA at compilation time. For example, these extensions can add the simulation of Cherenkov radiation or neutrinos, enable parallel computation of the shower simulation or adapt the simulation output to conform with the requirements of specific experiments.

2.2.2 Development of CORSIKA 8

Although originally developed only to provide simulations for the KASCADE experiment, CORSIKA evolved into a widely used program for air shower simulations. While updates for the interaction models are regularly released, new extensions for CORSIKA are rarely developed. One reason for the lack of new features is the complicated code structure that has originally been written without considering the possibility of new extensions. Instead, these extensions need to be developed to conform specifically with the existing code structure. Furthermore, CORSIKA is written in FORTRAN77 which, on the one hand, poses technical restrictions when developing new code, and on the other hand lacks a large user group compared to modern programming languages such as C++ or Python.

To overcome these existing obstacles, a new version of CORSIKA is being developed. With a code structure written from scratch in the programming language C++, CORSIKA 8 intends to provide a new shower simulation software focusing on flexibility and extensibility oriented towards the present use case of CORSIKA.

A description of the current status of the development of CORSIKA 8 is given by [39]. Furthermore, four building blocks, describing the very general code structure, are presented. These blocks are the particle stack, storing and giving access to all particle properties, the process sequence, describing all physical interactions, the transport code, responsible for the general propagation process as well as the environment that can be composed modularly by the user. One main feature of the CORSIKA 8 code is to provide the possibility to easily alter or replace functionalities of these building blocks. This allows CORSIKA 8 to be used not only as a simulation program for air showers but also as a framework for other simulation purposes.

2.2.3 The EGS4 computer code system

EGS4 (Electron Gamma Shower) is a standalone software package providing full Monte Carlo simulations of electromagnetic showers. The first version of EGS, developed at the Stanford Linear Acceleration Center, has been published in 1978 with EGS4 being released in 1985. EGS4 is capable of simulating the transport of electrons, positrons and photons in arbitrary geometries to obtain information on all secondary particles of an electromagnetic shower. Particles with energies beginning at the TeV range down to energies of only several keV can be treated by EGS. A detailed description of EGS4 is given by [36], a summary of the most important features of EGS4 and the changes made for its usage by CORSIKA is given as follows.

EGS4 is able to simulate the transport of particles in arbitrary media. This is made possible by the data preparation code PEGS4 which, based on cross section tables for atomic numbers between 1 and 100, creates the data necessary for the propagation in the requested medium which are then used by EGS4. After the tables for a specific medium have been created, EGS4 can be initialized either by receiving a monoenergetic particle to initiate an electromagnetic shower or by sampling an initial particle from a pre-defined distribution function. During the propagation of electrons and positrons, the original version of EGS4 takes into account bremsstrahlung effects, collision losses, Møller or Bhabha scattering, multiple scattering as well as annihilation (for positrons) while for photons, electron-positron pair production, Compton scattering as well as photonuclear interactions are considered.

For photon propagation, all interactions are sampled individually with the photon traversing in a straight line with constant energy between two separate interactions. When propagating charged leptons, EGS4 distinguishes between continuous and discrete interactions similar to the particle propagation in PROPOSAL as described in section 2.1.1. For every propagated particle, all produced secondary particles are stored and propagated as well, thus creating a full electromagnetic shower.

2.2.4 Usage of EGS4 in CORSIKA

Up to version seven, CORSIKA used EGS4 as an option to simulate the electromagnetic components of an atmospheric air shower. To conform with additional requirements imposed by CORSIKA, several changes were made to the original EGS4 code which are described in detail in [21].

Due to their importance for the muonic shower components, muon pair production by photons as well as the interaction of photons with protons and neutrons in

the atmosphere were added. To be able to describe interactions up to the highest energies correctly, existing cross section data have been extended up to 10^{20} eV. Furthermore, the LPM effect, affecting bremsstrahlung and pair production at very high energies, which is relevant for showers induced by high energy photons, has been integrated as well.

Since CORSIKA describes showers in a medium with an exponential density profile, the barometric density dependence of air influencing mean free path lengths as well as the density correction of ionization losses are relevant and have therefore been implemented in EGS4.

While EGS4 is natively able to treat the deflection of charged leptons in magnetic fields, approximations only valid for small deflection angles are used. To comply with this requirement, the propagation step size is limited in cases where the deflection due to the earth's magnetic field would be too large.

To optimize computing times, the maximum step size between two interactions of electrons or positrons is increased whenever possible. Furthermore, thinning measures are taken by removing particles from propagation if their probability to produce relevant secondary particles falls below a given threshold, preventing the calculation of irrelevant low-energy subshowers.

3 Integration of rare processes

When propagating particles, PROPOSAL considers ionization, bremsstrahlung, electron-positron pair production and photonuclear interactions. These four processes were originally chosen due to their quantitatively relevant contribution to the energy loss of muons, see figure 2.2. However, the polymorphic code structure of PROPOSAL allows for the simple implementation of additional interactions.

The following section describes the implementation of two rare processes, the production of muon pairs and the weak interaction of charged leptons, in PROPOSAL. While their contribution to the average energy loss is insignificant, they are able to produce qualitatively significant detector signatures for certain analyses as described individually in sections 3.1.3 and 3.2.3.

Definitions and numerical values of variables are, unless otherwise specified, listed, if necessary with their corresponding numerical values, in appendix B.

3.1 Muon pair production

The process of muon pair production is a rare process with a negligible contribution to the average energy loss of a propagated particle. However, the created signatures may be qualitatively relevant for neutrino observatories such as IceCube or underground detectors examining muons, see section 3.1.3 for a description of these signatures.

3.1.1 Theoretical description

Muon pair production describes the creation of a muon-antimuon pair by a particle in the field of an atomic nucleus Z , in case of an initial muon the reaction is

$$\mu^- + Z \rightarrow \mu^- + \mu^+ + \mu^- + Z.$$

A Feynman diagram in leading order for the process is shown in figure 3.1.

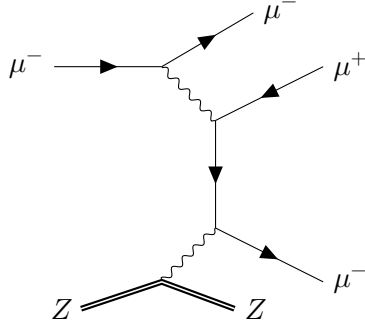


Figure 3.1: One possible Feynman diagram describing the creation of a muon pair by an ingoing muon.

The process has been described in [29] where a simplified analytical double differential cross section for muon pair production is given by

$$\frac{d^2\sigma}{dv d\rho} = \frac{2}{3\pi} (Z\alpha r_\mu)^2 \frac{1-v}{v} \Phi(v, \rho) \ln(X(E, v, \rho)) \quad (3.1)$$

with the relative energy loss v and the asymmetry parameter ρ defined by

$$v = \frac{E_+ + E_-}{E}, \quad \rho = \frac{E_+ - E_-}{E_+ + E_-} \quad (3.2)$$

and the energy of the produced (anti)muon E_\pm . The functions $\Phi(v, \rho)$ and $X(E, v, \rho)$ have the form

$$\begin{aligned} \Phi(v, \rho) = & [(2 + \rho^2)(1 + \beta) + \xi(3 + \rho^2)] \cdot \ln\left(1 + \frac{1}{\xi}\right) \\ & + \left[(1 + \rho^2) \left(1 + \frac{3}{2}\beta\right) - \frac{1}{\xi}(1 + 2\beta)(1 - \rho^2) \right] \cdot \ln(1 + \xi) \\ & - 1 - 3\rho^2 + \beta(1 - 2\rho^2) \end{aligned} \quad (3.3)$$

where X is given by

$$X = 1 + U(E, v, \rho) - U(E, v, \rho_{\max}) \quad (3.4)$$

with

$$U(E, v, \rho) = \frac{\frac{0.65m_\mu}{m_e} A^{-0.27} B Z^{-1/3}}{1 + \frac{2\sqrt{e}m_\mu^2 B Z^{-1/3}(1+\xi)(1+Y)}{m_e E v (1-\rho^2)}} \quad (3.5)$$

and with

$$\xi = \frac{v^2(1 - \rho^2)}{4(1 - v)}, \quad \beta = \frac{v^2}{2(1 - v)}, \quad Y = 12\sqrt{\frac{m_\mu}{E}}, \quad B = 183. \quad (3.6)$$

The approximative expression (3.1) takes into account the finiteness of the nucleus as well as screening effects of the nucleus by atomic electrons. A more precise formula for the differential cross section is given in [29] as well, however it includes multidimensional integrals that are hard to evaluate and is therefore not suited to be used here. Furthermore, (3.1) is chosen to have a discrepancy compared to the precise formula of below 10 % for all $E > 10^4$ MeV, the discrepancy of the derived total cross section is even below 3 % for $E > 3 \cdot 10^4$ MeV.

The kinematic limits of the process for v and ρ

$$v_{\min} = \frac{2m_\mu}{E}, \quad v_{\max} = 1 - \frac{m_\mu}{E}, \quad |\rho| \leq \rho_{\max} = 1 - \frac{2m_\mu}{vE}, \quad (3.7)$$

are easy to retrace by demanding the condition that all particles involved have to fulfill $E > m_{\text{rest}}$ at all times.

3.1.2 Implementation in PROPOSAL

The process of muon pair production is implemented as an optional, additional interaction in PROPOSAL. It is per default disabled in PROPOSAL and can be enabled by setting the keyword `mupair` in the configuration file to `MupairKelnerKokoulinPetrukhin` which is the parametrization that has been described in the previous section.

To obtain the single-differential cross section in v from (3.1), a numerical integration across the entire kinematic range of ρ

$$\frac{d\sigma}{dv} = \int_{\rho_{\min}}^{\rho_{\max}} \frac{d^2\sigma}{dv d\rho} d\rho \quad (3.8)$$

is performed in PROPOSAL. After sampling the relative energy loss v during propagation according to (2.18), the asymmetry parameter ρ is also sampled if the parameter `mupair_particle_output` has been set to `True`. In this case, (3.1) is used with a fixed $v = v^*$ to solve the integral equation

$$\left(\frac{d\sigma}{dv}(v^*) \right)^{-1} \int_{\rho_{\min}}^{\rho} \frac{d^2\sigma}{dv d\rho}(v^*) d\rho = \xi \quad (3.9)$$

for ρ where $\xi \in [0, 1]$ is a random number. An additional random number is used to decide on the sign of ρ , the muon energies then assigned are $E_{\pm} = vE \cdot (1 \pm \rho)$. In figure 3.2, the behavior of ρ for different muon energies and different v is shown. For high energies, the process tends to have a higher asymmetry ρ , especially when

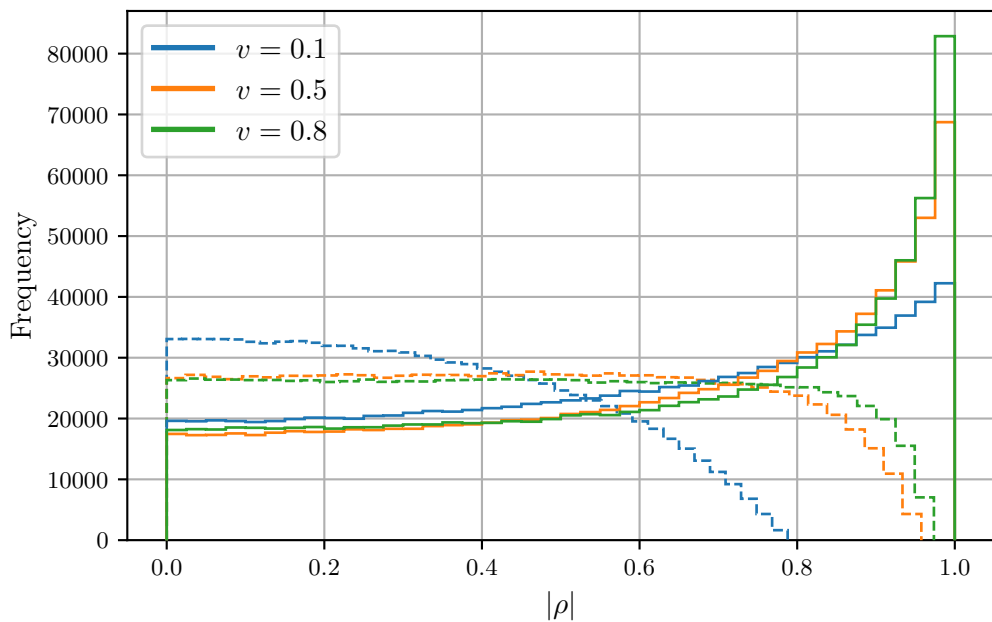


Figure 3.2: Histogram of $|\rho|$ for different v of muons in ice. For each v , ρ has been sampled 10^6 times. The dashed curves correspond to an initial muon energy of $E = 10^4$ MeV, the solid curves to $E = 10^9$ MeV.

a high relative energy loss is involved, while for lower energies, lower asymmetries are favored.

A comparison of the average energy loss in ice due to electron-positron pair production and muon pair production is shown in figure 3.3. Both functions behave similarly as they both grow linearly with E , still, the contribution from muon pair production is by about three orders of magnitudes lower for high energies and even lower for small energies. This observation shows that the process is negligible for the energy loss for the muon which is especially a result of the difference between the muon mass and the electron mass since

$$\frac{\sigma_{\mu\text{pair}}}{\sigma_{e\text{pair}}} \propto \frac{r_\mu^2}{r_e^2} = \frac{m_e^2}{m_\mu^2} \approx 2 \cdot 10^{-5}.$$

The average energy loss due to muon pair production compared to the energy loss due to other interactions in PROPOSAL is shown in figure 3.7.

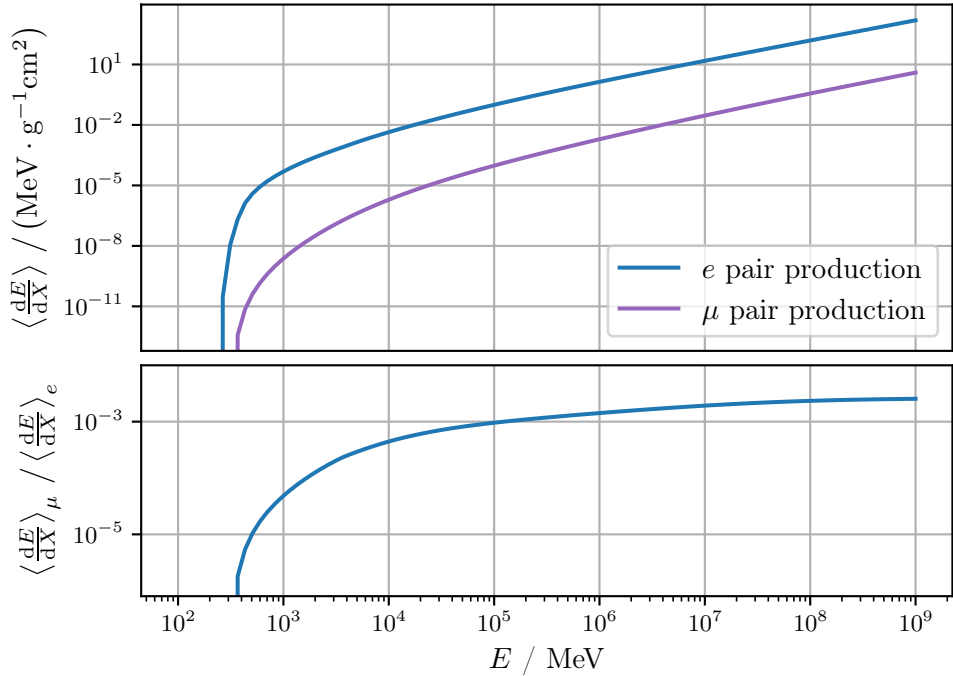


Figure 3.3: Comparison of the average continuous energy losses of muons in ice due to electron-positron pair production [27, 33] and muon pair production. No energy cuts are applied in this plot, hence this plot represents the case where all losses are treated continuously.

Figure 3.4 shows a secondary particle spectrum where muon pair production is enabled. The contribution from muon pair production tends to be distributed among all secondary energies but is, as expected, suppressed compared to contributions from other interactions. Figure 3.5 illustrates the contribution to the secondary particle spectrum if the muons produced by muon pair production are further propagated. Here, it can be seen that the influence of muon pair production on the shape of the secondary particle spectrum appears to be negligible.

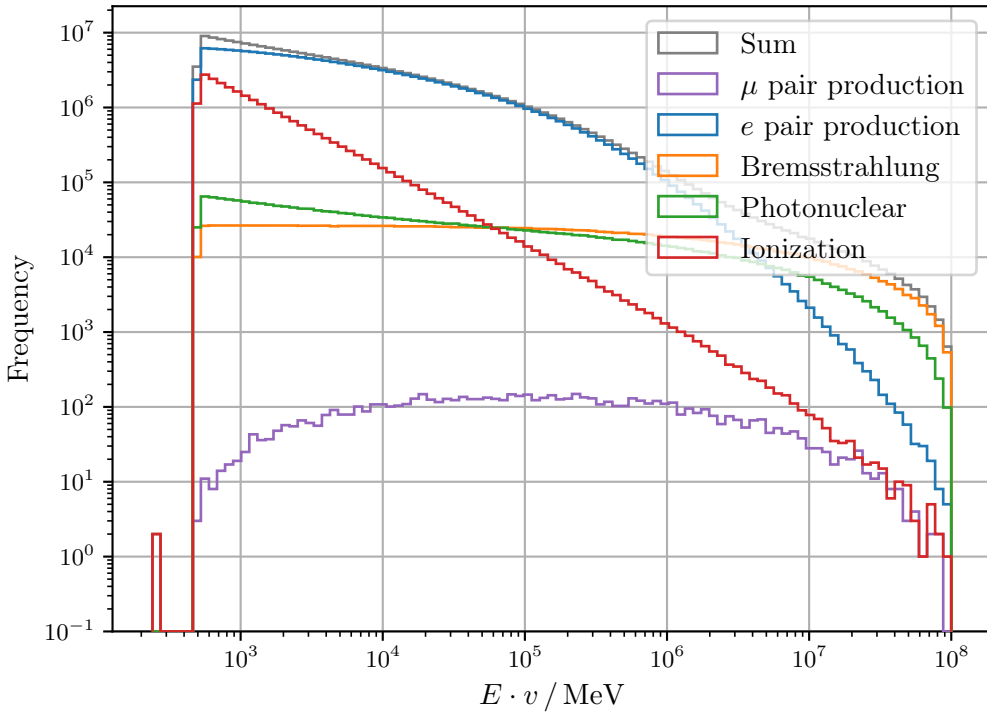


Figure 3.4: Secondary particle spectrum for 10^5 muons with an initial energy of 10^8 MeV, propagated in ice. Muon pair production is enabled. The histogram shows the frequency of the stochastic losses during propagation, classified by the type of energy loss. The energy cuts applied here are $e_{\text{cut}} = 500$ MeV, $v_{\text{cut}} = 0.05$.

3.1.3 Significant detector signatures

As already described and shown in section 3.1.2, the contribution of muon pair production to the overall energy loss of muons is negligible. However, for detectors interested in muon events, the effects of muon pair production may portray a source of significant signatures. In the following, a group of muons moving into almost the

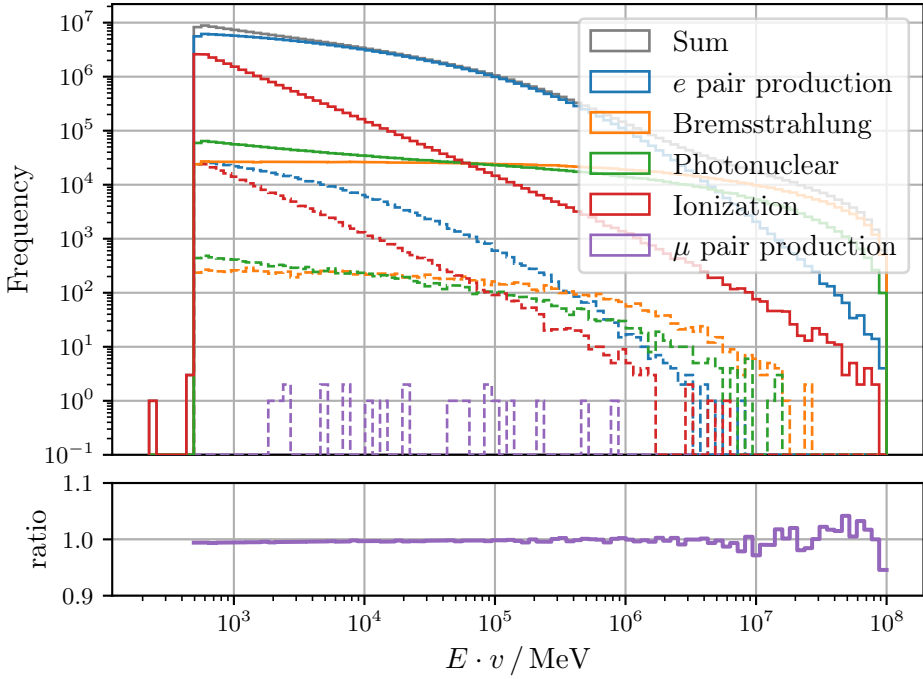


Figure 3.5: Secondary particle spectrum for 10^5 muons with an initial energy of 10^8 MeV, propagated in ice. The solid lines in the histogram show the secondary particle spectrum where muon pair production is disabled. The dashed lines show the additional particle spectrum induced by muons that are created if muon pair production is enabled. The energy cuts applied here are $e_{\text{cut}} = 500$ MeV, $v_{\text{cut}} = 0.05$. The ratio plot in the lower part of the figure shows the difference between the sum of all secondary particles if muon pair production is disabled compared to the sum of all secondary particles if muon pair production is enabled and the produced muons are propagated as well.

same direction with only a small separation is called a muon bundle. The origin of such a bundle can be muon pair production, in this case, the bundle consists of three muons.

IceCube event signatures

Due to resolution effects, the IceCube detector is unable to identify the muons in a bundle as individual muon signatures [3]. However, the signature of a single muon traversing the detector is different from a muon bundle originating from muon pair production with the same sum of energy. The signature of a high-energetic muon in IceCube is often characterized by a dominating high-energetic stochastic energy loss creating a spherical signature. In a muon bundle, each muon with only a fraction of the total energy produces smaller stochastic losses. Since the stochastic losses of the individual muons in the bundle are independent of each other, the resulting signature is more homogeneous and the energy loss per distance of a bundle is more uniform compared to the energy loss per distance of a single muon with the same total energy [17].

Background for muon bundles in extensive air showers

Underground detectors observing muons originating from extensive air showers can use the information about muon bundles created in these air showers to learn about the cosmic ray composition and hadronic interaction models. This is done by comparing the frequency and multiplicity of muon bundles as well as the muon separation measured in experiments with the predictions from Monte Carlo studies. In [34], the authors describe this procedure in more detail and point out a possible background from muon pair production.

While about 1 % to 10 % of the observed muons are part of muon bundles induced in the air shower, these bundles can also be produced due to muon pair production in rock or water above the underground detector. According to calculations in [34], these bundles induced by muon pair production can portray a background of up to 10 % compared to the conventional bundles in the showers, although more exact calculations have to be performed individually for each experiment considering its specific geometric properties. Due to the difference in the distance between the creation and observation point of the muon bundle, both effects can be separated statistically by examining the separation distance in the bundle. The separation of muon bundles due to muon pair production is mostly below 1 m while for muon bundles induced in air showers, only a small percentage of the muon bundles have such a small separation [34].

3.2 Weak interaction of charged leptons

The process called weak interaction in PROPOSAL refers to the conversion of a charged lepton to a neutrino under exchange of a W boson, i.e. a charged current weak interaction. This interaction is highly suppressed compared to other processes. However, the produced signature can be of importance, for example as a background for tau neutrino searches as described in section 3.2.3.

3.2.1 Theory and data description

The process of interest

$$l + N \rightarrow \nu_l + X \quad (3.10)$$

with a charged lepton l , the corresponding neutrino ν_l , the initial nucleon N and the hadronic final state X describes the conversion of a charged lepton to a neutrino under exchange of a W boson. This specific process is related to the interaction of an anti-neutrino under exchange of a W boson, i.e.

$$\bar{\nu}_l + N \rightarrow \bar{l} + X, \quad (3.11)$$

via crossing symmetry¹ as depicted in figure 3.6 [20]. Since the kinematics of both

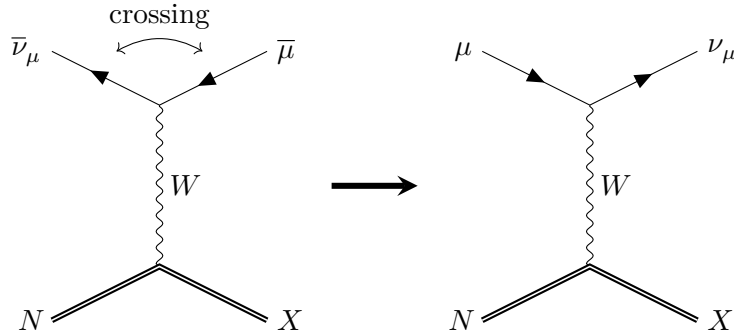


Figure 3.6: Feynman diagrams of lepton interactions under exchange of a W boson and its connection via crossing symmetry.

processes are identical, the differential cross sections are also identical except for a prefactor of $1/2$,

$$d\sigma(l + N \rightarrow \nu_l + X) = \frac{1}{2} d\sigma(\bar{\nu}_l + N \rightarrow \bar{l} + X). \quad (3.12)$$

¹The argument of crossing symmetry is identical when switching all particles with their corresponding antiparticles, i.e. the process $\bar{l} + N \rightarrow \bar{\nu}_l + X$ is related to $\nu_l + N \rightarrow l + X$.

3.2 Weak interaction of charged leptons

Due to averaging over all possible initial states and summing over all possible final states when evaluating Feynman diagrams, the prefactor $1/2$ must be taken into account since the muon can both be left-handed and right-handed while neutrinos are only observed in a left-handed state (and antineutrinos in a right-handed state) [42].

Tabulated numerical values for the differential cross section describing the conversion of a neutrino to a charged lepton, i.e. the process (3.11), are available from [12]. By using crossing symmetry, these data can directly be used to describe the conversion of a charged lepton to a neutrino, i.e. (3.10), which is the process of interest in PROPOSAL.

The cross sections for interactions of leptons with hadrons can be derived under the use of parton distribution functions which describe the probability to find a specific parton (quark or gluon) with a given fraction x of the nucleon's momentum when the momentum transfer is given by Q^2 . To make predictions for the (anti)neutrino charged current cross sections, the authors of [12] performed next-to-leading order calculations and used the HERAPDF1.5 data set which provides the parton distribution functions based on deep-inelastic scattering measurements performed at the HERA experiment from 2003 to 2007 [11].

The values for $d\sigma/dv$ are provided as two-dimensional tables in E and v with 100 entries in E and, for each energy, 110 entries in v . Here, v describes the fraction of the initial lepton energy E lost to the nucleon. Tables are available for an ingoing neutrino or an ingoing antineutrino and for a proton or a neutron as a nucleon involved in the interaction. The ranges of the tabulated values are $10 \text{ GeV} \leq E \leq 10^{12} \text{ GeV}$ and $v_{\min} < v < 1$ in equal, logarithmic intervals. The lower limit of v has been set to

$$v_{\min} = \frac{Q_{\min}^2}{s}, \quad s = 2Em + m^2, \quad Q_{\min}^2 = 1 \text{ GeV}^2, \quad (3.13)$$

with the mass of the involved nucleon m and the center-of-mass energy \sqrt{s} . For values where $Q^2 < Q_{\min}^2$, the underlying theory of quantum chromodynamics can no longer be treated perturbatively, meaning that the predictions for the cross sections are not reliable in this kinematic range [12].

3.2.2 Implementation in PROPOSAL

The weak interaction process is by default disabled in PROPOSAL and can optionally be enabled by setting the keyword `weak` in the configuration file to `CooperSarkarMertsch` which is the parametrization described in the previous section.

For a component with an atomic number Z and a mass number A , the differential cross section is combined from the given tables to be

$$\frac{d\sigma}{dv} \propto Z \cdot \frac{d\sigma_p}{dv} + (A - Z) \cdot \frac{d\sigma_n}{dv} \quad (3.14)$$

where the subscript refers to the nucleon involved in the interaction (p for proton and n for neutron). PROPOSAL then uses a two-dimensional interpolation routine to obtain a continuous differential cross section from the discrete table values.

In contrast to previously described processes, the weak interaction is a catastrophic loss meaning that the initial particle ceases to exist since it is converted to a different type of particle during the interaction. Therefore, treating a process with this signature continuously as described in section 2.1.1 would be unphysical, meaning that there is no contribution to the continuous loss in (2.6) from these interactions. Additionally, all interactions with catastrophic losses are treated stochastically by neglecting the energy cut in (2.17) and (2.18). Instead, the lower integral limit is set to v_{\min} . After a weak interaction, PROPOSAL returns the produced neutrino as well as the energy transfer to the nucleon and stops the particle propagation.

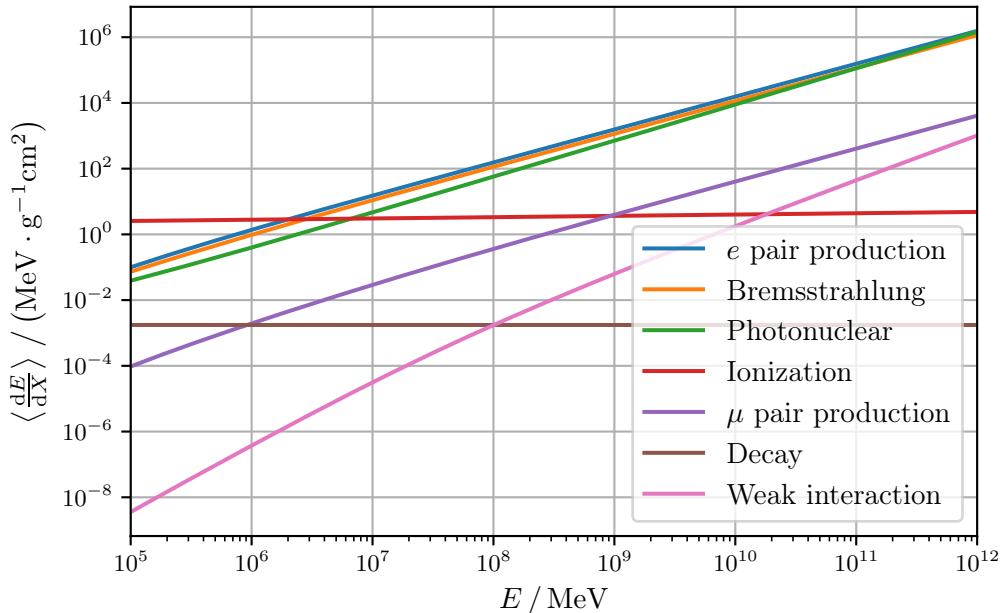


Figure 3.7: Comparison of the average energy loss of muons in ice due to weak interactions in comparison to other interactions. Note that losses due to weak interactions are always stochastic, the average energy loss is calculated by taking into account that the muon loses all its energy during a weak interaction event.

Figure 3.7 shows the average energy loss due to weak interactions compared to the average energy loss due to other processes. For high energies, the average energy loss due to weak interactions is suppressed by three orders of magnitude compared to other default processes in PROPOSAL with an even higher suppression for lower energies. Therefore, its quantitative contribution to the average energy loss is entirely negligible.

3.2.3 Significant detector signatures

As described in the previous section, the weak interaction process is highly suppressed and therefore negligible in its contribution to the average energy loss of a charged lepton. However, under certain conditions, the detector signature of the process could be significant for searches of tau neutrinos, for example in the IceCube neutrino observatory [42].

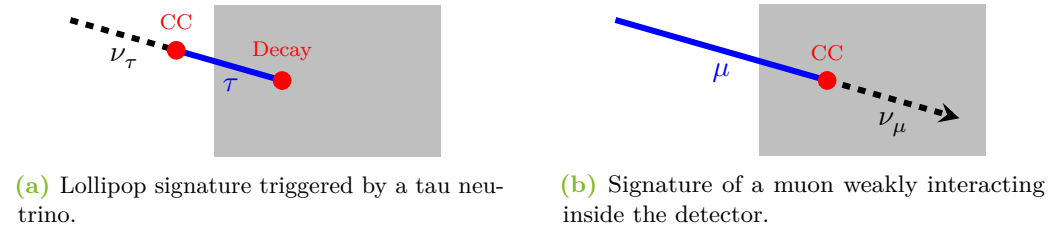


Figure 3.8: Illustrations of two signatures relevant for tau neutrino searches. The detector volume is drawn gray, hadronic cascades are drawn as a red dot, observable tracks are drawn as blue lines and tracks that are not directly observable are drawn as a black, dotted line.

One possible signature hinting at a tau neutrino event called the "lollipop" signature is illustrated in figure 3.8a. Here, a tau neutrino moving towards the detector interacts via a charged current and is being converted to a tau lepton [13]. The tau lepton then enters the detector, leaving behind an observable track of Cherenkov light emerging from the tau itself and the created secondary particles. Due to its short lifetime, the created tau can only reach the detector if its energy is high enough since the average tau decay length scales with energy as 5 cm/TeV [1]. If the tau decays to a hadron inside the detector, a hadronic cascade is generated at the end of the track, giving the signature its characteristic name.

This tau neutrino signature can be imitated by the event shown in figure 3.8b. In this case, a muon, leaving behind a track, enters the detector where it weakly interacts and is therefore converted to a neutrino. Due to the energy transfer to the involved nucleus in the weak interaction, the process creates a hadronic cascade

comparable to the cascade of a hadronic tau decay. Since the created neutrino is not observable, the overall signature where a track starts outside the detector and ends in a hadronic cascade can be confused with the lollipop signature from figure 3.8a. However, the tracks from both signatures behave differently since the energy loss per distance of a muon is higher than the energy loss of a tau. To have a similar track signature, the tau involved needs to have an energy that is about 6 to 11 times higher than the energy of a corresponding muon [42].

It follows that analyses searching for lollipop signatures have to consider the weak interaction as a possible background. According to approximative calculations in [42] based on the properties of the IceCube detector, the expected rate of false lollipop events due to atmospheric muons undergoing weak interactions is about $2 \cdot 10^{-2} / \text{yr}$. This, together with further approximative calculations for real lollipop signatures from tau neutrino events, corresponds to a possible background of 10 %. However, further effects such as event selection efficiency (assumed to be perfect in this calculation) or a detailed detector simulation were not taken into account but need to be evaluated when conducting a detailed analysis.

4 Propagation of electromagnetic showers

As described in section 2.2, CORSIKA 7 uses the software package EGS4 to simulate the electromagnetic components of extensive air showers. However, the development of the original EGS code ended with the release of EGS4, although other groups continued working on the given code foundation [24, 26].

For the currently developed new version CORSIKA 8, up-to-date models to describe the electromagnetic shower components are needed. As an actively maintained propagation program written in a modern programming language, PROPOSAL represents a possible choice for this purpose. As a requirement, PROPOSAL needs to be able to propagate electrons, positrons and photons.

In the following section, the measures taken to improve the propagation of electrons and positrons as well as the measures taken to realize the propagation of photons are described. Furthermore, as a proof of concept, simulations of photon-induced electromagnetic showers with PROPOSAL using the newly implemented cross sections are presented.

Definitions and numerical values of variables are, unless otherwise specified, listed, if necessary with their corresponding numerical values, in appendix B.

4.1 Electron and positron propagation in PROPOSAL

Although most processes relevant for electron and positron propagation are already implemented in PROPOSAL, the included cross sections are optimized for muon and tau propagation, requiring some parametrizations to be adapted.

The currently used parametrization of ionization doesn't provide correct results when applied to electrons and positrons, a correct parametrization is therefore implemented as described in section 4.1.1. Since bremsstrahlung effects are dominant for electrons and positrons, an optimized parametrization, as described in section 4.1.2, is added to PROPOSAL. For positrons, annihilation with atomic electrons is a new interaction that is not described by other processes, the treatment of electron-positron annihilation in PROPOSAL is presented in section 4.1.3.

4.1.1 Ionization

Ionization describes the inelastic collision of a particle with atomic electrons, leading to an energy loss of the primary particle. For heavy, charged particles, the average energy loss due to ionization is given by the Bethe formula. PROPOSAL uses a modified Bethe formula, taking into account density correction effects, to describe the ionization losses for muon and tau leptons [32, 41, 44]. However, the Bethe formula can't be applied for electrons and positrons due to their lower mass as well as the indistinguishability of incoming electrons with atomic electrons [8]. Therefore, a separate treatment of the ionization losses for electrons and positrons is necessary.

Theoretical description

For energy transfers ν significantly greater than the atomic excitation levels, the atomic electrons can be considered as free and in rest. In this case, the ionization process is essentially electron-electron scattering ($e^- + e^- \rightarrow e^- + e^-$), known as Møller scattering, or positron-electron scattering ($e^+ + e^- \rightarrow e^+ + e^-$), known as Bhabha scattering. The two Feynman diagrams contributing in leading order for Møller scattering are shown in figure 4.1, the differential cross section [40] is given by

$$\left(\frac{d\sigma}{dv} \right)_- = \frac{2\pi r_e^2 Z\gamma}{\beta^2(\gamma-1)^2} \left[\frac{(\gamma-1)^2}{\gamma^2} + \frac{1}{\epsilon} \left(\frac{1}{\epsilon} - \frac{2\gamma-1}{\gamma^2} \right) + \frac{1}{1-\epsilon} \left(\frac{1}{1-\epsilon} - \frac{2\gamma-1}{\gamma^2} \right) \right] \quad (4.1)$$

with

$$\epsilon = \frac{vE}{E-m_e}, \quad \gamma = \frac{E}{m_e}, \quad \beta = \sqrt{1 - \frac{1}{\gamma^2}}, \quad v_{\max} = \frac{1}{2} - \frac{m_e}{2E}. \quad (4.2)$$

For Bhabha scattering, the two Feynman diagrams contributing in leading order are shown in figure 4.2 and the differential cross section [40] is given by

$$\left(\frac{d\sigma}{dv} \right)_+ = \frac{2\pi r_e^2 Z\gamma}{(\gamma-1)^2} \left[\frac{1}{\beta^2\epsilon^2} - \frac{B_1}{\epsilon} + B_2 - B_3\epsilon + B_4\epsilon^2 \right] \quad (4.3)$$

with

$$B_1 = 2 - y^2, \quad B_2 = (1 - 2y)(3 + y^2), \\ B_3 = (1 - 2y)^2 + (1 - 2y)^3, \quad B_4 = (1 - 2y)^3,$$

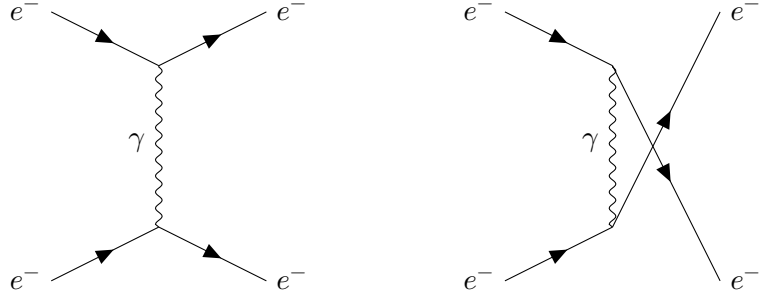


Figure 4.1: Feynman diagrams in leading order for Møller scattering. The t -channel diagram is shown on the left, the u -channel diagram is shown on the right.

and

$$y = \frac{1}{\gamma + 1}, \quad v_{\max} = 1 - \frac{m_e}{E}.$$

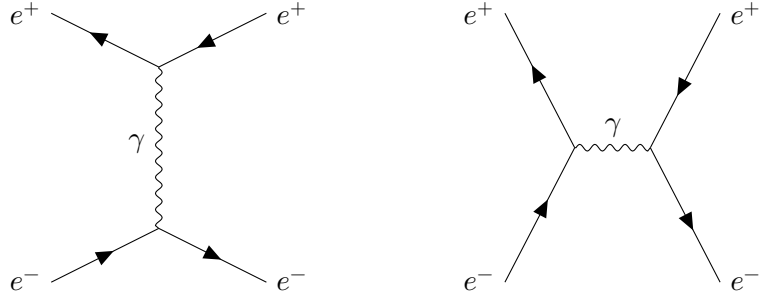


Figure 4.2: Feynman diagrams in leading order for Bhabha scattering. The diagram describing the scattering process is shown on the left, the diagram describing the annihilation process is shown on the right.

For energy transfers ν in the same order of magnitude as the atomic excitation levels, the explicit excitation probabilities $p(E, v)$ need to be considered. Defining a threshold transfer energy ν_{thres} that is above the atomic excitation levels but below the energy cut in PROPOSAL, the continuous energy loss per distance due to ionization can be written as

$$-\left(\frac{dE}{dX}\right)_{\pm} \propto \int_0^{\nu_{\text{thres}}/E} v \cdot p(E, v) dv + \int_{\nu_{\text{thres}}/E}^{v_{\text{cut}}} v \cdot \left(\frac{d\sigma}{dv}\right)_{\pm} dv. \quad (4.4)$$

For an appropriate value of ν_{thres} , certain approximations can be applied where (4.4)

yields [40]

$$-\left(\frac{dE}{dX}\right)_{\pm} = \frac{2\pi r_e^2 m_e}{\beta^2} \left[\log\left(\frac{2m_e(\tau+2)}{I}\right) + F^{\pm}(\tau, \Delta) - \delta \right], \quad (4.5)$$

also known as the Berger-Seltzer formula [24], with

$$\tau = \gamma - 1, \quad \Delta = \min \left[\frac{v_{\max} E}{m_e}, \frac{v_{\text{cut}} E}{m_e} \right], \quad (4.6)$$

the mean ionization energy of the medium I and the contribution from the density correction δ , described in detail in [32]. Furthermore, $F^{\pm}(\tau, \Delta)$ differs for electrons (F^-) and positrons (F^+) and is defined by

$$F^+(\tau, \Delta) = \ln(\tau\Delta) - \frac{\beta^2}{\tau} \left[\tau + 2\Delta - \frac{3\Delta^2}{2} - (\Delta - \frac{\Delta^2}{3})y^2 - (\frac{\Delta^2}{2} - \frac{\tau\Delta^3}{3} + \frac{\Delta^4}{4})y^3 \right], \quad (4.7)$$

$$F^-(\tau, \Delta) = -1 - \beta^2 + \ln((\tau - \Delta)\Delta) + \frac{\tau}{\tau - \Delta} + \frac{1}{\gamma^2} \left[\frac{\Delta^2}{2} + (2\tau + 1) \log\left(1 - \frac{\Delta}{\tau}\right) \right]. \quad (4.8)$$

Implementation in PROPOSAL

The ionization cross sections for electrons and positrons described above can be used in PROPOSAL by setting the keyword `ioniz` in the configuration file to `IonizBergerSeltzerMoller` to use the parametrization for electrons or `IonizBergerSeltzerBhabha` to use the parametrization for positrons.

To take into account the atomic excitation levels relevant for small energy transfers, the Berger-Seltzer formula, i.e. (4.4), is used when calculating continuous ionization losses. When sampling stochastic losses, the differential cross section for Møller scattering (4.1), respectively the differential cross section for Bhabha scattering (4.3), is used directly since the contributions from small energy transfers are negligible here.

Figure 4.3 shows the differences in the continuous ionization loss for electrons and positrons when using the appropriate Berger-Seltzer formula compared to the Bethe formula. It can be seen that, neglecting NLO corrections, the difference is up to 5 % for small energies. Furthermore, the Berger-Seltzer formula, compared to

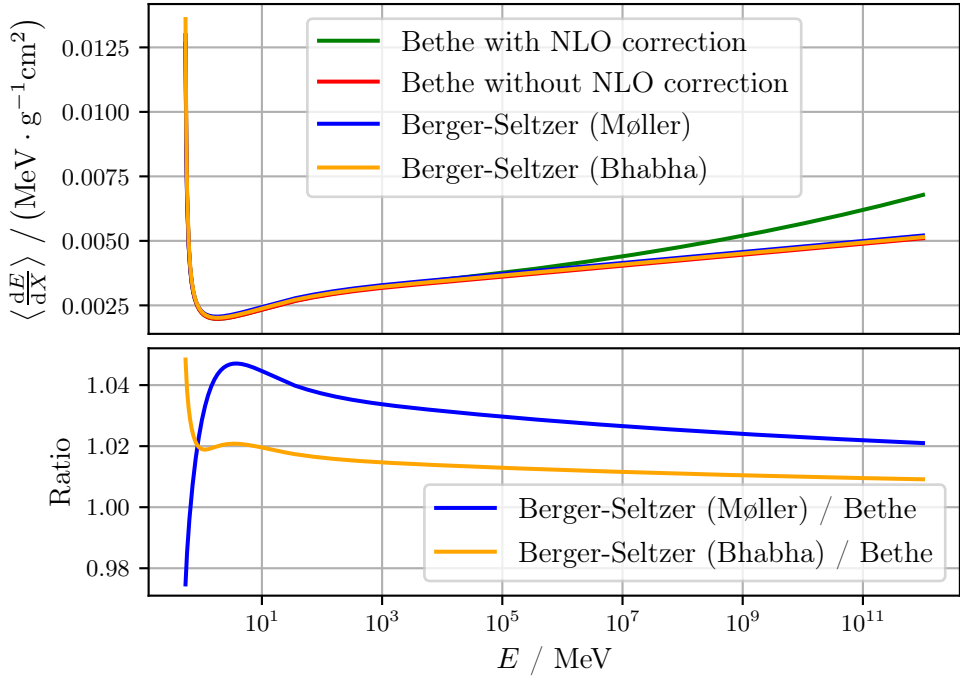
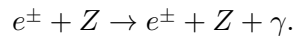


Figure 4.3: Average energy loss of electrons and positrons in air due to ionization. Note that the Bethe formula is, unlike the Berger-Seltzer formula, identical for electrons and positrons. The default Bethe parametrization used in PROPOSAL includes NLO inelastic bremsstrahlung corrections [32]. For an easier comparison to the Berger-Seltzer formula (which does not consider NLO corrections), the Bethe formula without NLO corrections has been calculated as well. In the lower half of the figure, this version of the Bethe formula is compared to the Berger-Seltzer formulas.

the Bethe formula which is independent of the particle charge, takes differences between ionization energy losses of electrons and positrons into account. While the contribution from atomic excitation levels is, as a good approximation, identical for electrons and positrons [40], the contribution from high energy transfers differs. Here, if the ingoing particle is an electron, it is indistinguishable from the atomic electron after the ionization process. Therefore, the electron with the higher energy after the interaction is by definition the initial particle. However, a positron as an ingoing particle is always distinguishable from the atomic electron and can therefore be the particle with the lower energy after the interaction.

4.1.2 Bremsstrahlung

Bremsstrahlung describes the energy loss of a charged particle in the field of an atomic nucleus Z where a photon is emitted, i.e.



Since the process has a m^{-2} mass dependency, bremsstrahlung is the dominant interaction for high energy electrons and positrons. It is therefore relevant to provide an accurate description of the bremsstrahlung cross section.

For electrons with high energies, [32] recommends the usage of the Complete Screening parametrization which has already been implemented in PROPOSAL. This ultra-relativistic cross section, given and described by [45], uses Coulomb corrections as well as the assumption that the screening of the Coulomb field of the nucleus by the atomic electron cloud is maximal, which is an appropriate approximation for high-energy electrons.

EGS uses an alternative parametrization of the bremsstrahlung interaction, including empirical corrections for low energies [24]. This parametrization is implemented in PROPOSAL to examine the differences between the cross sections provided by PROPOSAL and EGS as well as effects from low energy corrections.

Theoretical description

The bremsstrahlung cross section provided by EGS, which is described in detail by [24], is split into a high-energy and a low-energy part with a discrete cut at 50 MeV.

4.1 Electron and positron propagation in PROPOSAL

For $E > 50$ MeV, the ultra-relativistic differential cross section, comparable to the Complete Screening parametrization in PROPOSAL, is given by

$$\frac{d\sigma}{dv} = \frac{Z(Z + \xi(Z))r_e^2\alpha}{v} \left[(2 - 2v + v^2) \left(\Phi_1(x) - \frac{4}{3} \ln(Z) - 4f_c(Z) \right) - \frac{2}{3}(1-v) \left(\Phi_2(x) - \frac{4}{3} \ln(Z) - 4f_c(Z) \right) \right] \quad (4.9)$$

with

$$x = 136Z^{-1/3} \frac{2\delta}{m_e}, \quad \delta = \frac{m_e^2 v}{2E(1-v)}. \quad (4.10)$$

The functions $\Phi_1(x)$, $\Phi_2(x)$ describe the screening effects and are given by

$$\Phi_1(x) = \begin{cases} 20.867 - 3.242x + 0.625x^2 & \text{if } x \leq 1, \\ 21.12 - 4.184 \ln(x + 0.952) & \text{if } x > 1, \end{cases} \quad (4.11)$$

$$\Phi_2(x) = \begin{cases} 20.029 - 1.930x - 0.086x^2 & \text{if } x \leq 1, \\ 21.12 - 4.184 \ln(x + 0.952) & \text{if } x > 1, \end{cases} \quad (4.12)$$

which is an analytical approximation of the Thomas-Fermi form factors. Furthermore, $f_c(Z)$ describes the Coulomb correction and is approximated in an analytical form by

$$f_c(Z) \approx a^2 \left[\frac{1}{1+a^2} + 0.20206 - 0.0369a^2 + 0.0083a^4 - 0.002a^6 \right] \quad (4.13)$$

with $a = \alpha Z$. The parameter

$$\xi(Z) = \frac{L'_{\text{rad}}(Z)}{L_{\text{rad}}(Z) - f_c(Z)} \quad (4.14)$$

with the radiation logarithms

$$L'_{\text{rad}} = \begin{cases} \ln(1194Z^{-2/3}) & \text{if } Z > 4, \\ 5.924 & \text{if } Z = 4, \\ 5.805 & \text{if } Z = 3, \\ 5.621 & \text{if } Z = 2, \\ 6.144 & \text{if } Z = 1, \end{cases} \quad (4.15)$$

$$L_{\text{rad}} = \begin{cases} \ln(184.15Z^{-1/3}) & \text{if } Z > 4, \\ 4.710 & \text{if } Z = 4, \\ 4.740 & \text{if } Z = 3, \\ 4.790 & \text{if } Z = 2, \\ 5.310 & \text{if } Z = 1, \end{cases} \quad (4.16)$$

accounts for atomic electron effects.

For $E < 50$ MeV, the differential bremsstrahlung cross section is given by

$$\frac{d\sigma}{dv} = \frac{A'(E, Z)Z(Z + \xi(Z))r_e^2\alpha}{v} \left[(2 - 2v + v^2) \left(\Phi_1(x) - \frac{4}{3} \ln(Z) \right) - \frac{2}{3}(1 - v) \left(\Phi_2(x) - \frac{4}{3} \ln(Z) \right) \right] \quad (4.17)$$

where a density correction factor $A'(E, Z)$ has been introduced. This factor $A'(E, Z)$ rescales the differential cross section to be in agreement with the empirical average energy losses per distance from [7], the detailed procedure to obtain this correction is described in [14]. It should be noted that this factor is only a normalization factor and is therefore not affecting the shape of the energy loss distribution itself.

Implementation in PROPOSAL

To use the bremsstrahlung cross section described above in PROPOSAL, the keyword `brems` in the configuration file can be set to `BremsElectronScreening`.

The values for $A'(E, Z)$ are provided as a two-dimensional table in $\ln(Z)$ and E with 14 entries in $\ln(Z)$ and, for each $\ln(Z)$, 115 entries in E . PROPOSAL uses a two-dimensional interpolation routine to obtain the correction factor for an arbitrary (Z, E) from the discrete table values.

Figure 4.4 shows a comparison of the average energy loss for electrons¹ loss due to bremsstrahlung when using different parametrizations. For very high energies, all parametrizations yield comparable results. However, differences exceeding a factor of 1.5 can be seen for lower energies, especially in the domain of several MeV. It is particularly noticeable that the results from the Electron Screening parametrization are in better agreement with the Andreev Bezrukov Bugaev parametrization than the Complete Screening parametrization, although the latter has been recommended for (high energy) electrons.

Furthermore, a discontinuity at 50 MeV when using the Electron Screening parametrization is notable. This behavior results from the fact that the correction factor $A'(E, Z)$ is set to 1 for $E > 50$ MeV although this approximation is invalid according to empirical data implying that $A'(E, Z) \neq 1$ for energies above the cut. A smoothing of the correction parameter around 50 MeV could remove the unphysical

¹Regarding only leading order calculations in α , the bremsstrahlung cross section is identical for electrons and positrons [45].

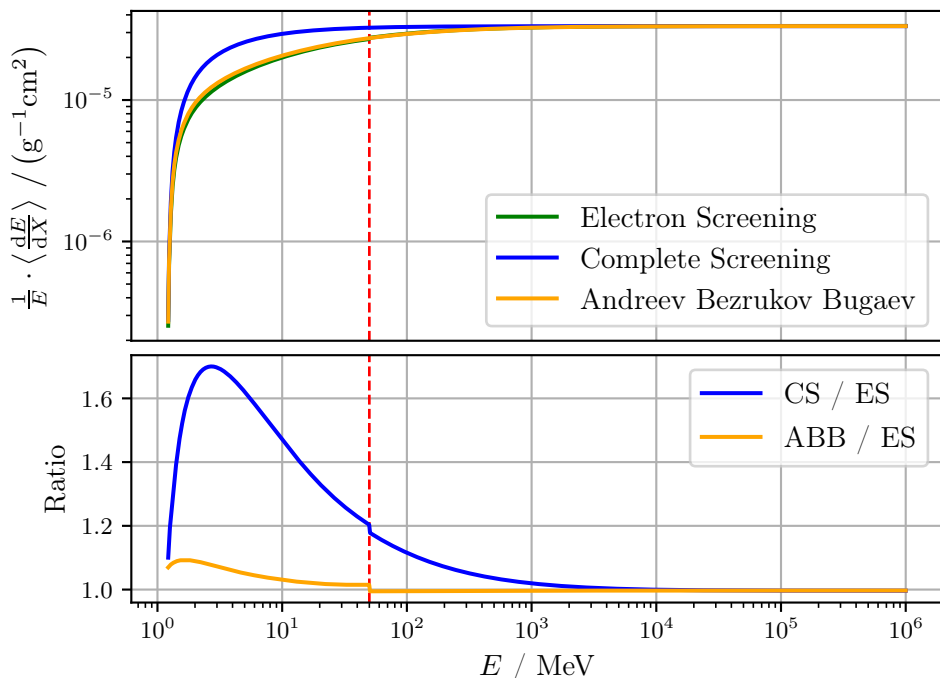


Figure 4.4: Comparison of the average energy loss of electrons in air due to bremsstrahlung between the parametrization adapted from EGS (Electron Screening) and two alternative parametrizations (Complete Screening, Andreev Bezrukov Bugaev). The dashed red line highlights the cut applied in the Electron Screening parametrization between the high-energy part and the low-energy part.

discontinuity, however, such a method would be arbitrary to a certain extent. Alternatively, using a differential cross section applicable for all energies without relying on empirical correction factors would be preferable for PROPOSAL.

4.1.3 Electron-positron annihilation

Electron-positron annihilation, only called annihilation in the further course of this section, describes the collision of a positron with an atomic electron where both particles annihilate and a pair of photons is created, i.e the process

$$e^+ + e^- \rightarrow \gamma + \gamma,$$

which is therefore only relevant when propagating positrons. The Feynman diagram describing this process in leading order is shown in figure 4.5.

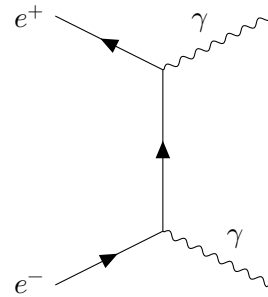


Figure 4.5: Feynman diagram in leading order for electron-positron annihilation.

Theoretical description

Under the assumption that the atomic electron is initially free and at rest, which is an appropriate approximation for positrons with energies high compared to atomic binding energies, the differential annihilation cross section is described by the Heitler formula [23] and given by [24]

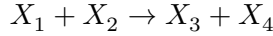
$$\frac{d\sigma}{d\epsilon} = \frac{\pi r_e^2}{\gamma - 1} \frac{1}{\epsilon} \left[1 + \frac{2\gamma}{(\gamma + 1)^2} - \epsilon - \frac{1}{(\gamma + 1)^2} \frac{1}{\epsilon} \right]. \quad (4.18)$$

Here, γ and ϵ are defined by

$$\gamma = \frac{E}{m_e}, \quad \epsilon = \frac{E_{\gamma,1}}{E + m_e},$$

with the energy of the initial positron E and the energy $E_{\gamma,1}$ of one of the created photons. Here, ϵ describes the ratio of the energy transfer to one of the created photons to the available energy, i.e. the positron energy and the mass of the atomic electron.

Since annihilation describes a two-body interaction, the kinematics of the final state are fully determined for a given E and ϵ . A general two-body interaction can be described by the process



with the corresponding energies E_i , masses m_i and absolute momenta p_i of the particles involved. Applying the conservation of four-momentum (i.e. conservation of energy and conservation of 3-space momentum) leads to the relation [24]

$$\cos(\theta_3) = \frac{m_4^2 - m_1^2 - m_2^2 - m_3^2 + 2(E_1 + m_2)E_3 - 2E_1m_2}{2p_1p_3} \quad (4.19)$$

for the frame where X_2 is in rest with the angle θ_3 between the incident particle X_1 and the final particle X_3 . For annihilation, using

$$\begin{aligned} E_1 &= E, & m_1 &= m_2 = m_e, \\ E_2 &= m_e, & m_3 &= m_4 = 0, \\ E_3 &= \epsilon(E + m_e), \end{aligned}$$

yields the relation

$$\cos(\theta_3) = \frac{\epsilon(\gamma + 1) - 1}{\epsilon\sqrt{\gamma^2 - 1}} \quad (4.20)$$

as well as, using a similar calculation, the relation

$$\cos(\theta_4) = \frac{(1 - \epsilon)(\gamma + 1) - 1}{(1 - \epsilon)\sqrt{\gamma^2 - 1}}. \quad (4.21)$$

Furthermore, setting $\cos(\theta_3) = \pm 1$ in 4.20 yields the kinematic limits for ϵ

$$\epsilon_{\max/\min} = \frac{1}{2} \pm \frac{1}{2}\sqrt{\frac{\gamma - 1}{\gamma + 1}}. \quad (4.22)$$

Implementation in PROPOSAL

The annihilation cross section described in the previous section, which is per default disabled in PROPOSAL, can be enabled by setting the keyword `annihilation` in the configuration file to `AnnihilationHeitler`.

The annihilation process is a catastrophic loss, similar to the weak interaction whose treatment is described in section 3.2.2, since the initial positron ceases to exist after the interaction. Accordingly, treating this process as continuous would be unphysical. Instead, the annihilation interaction is always stochastic and the relative energy loss of the initial positron is always $v = 1$ since all energy is transferred to the created photon pair. This requires adjustments to the simulation of the stochastic energy loss in the propagation algorithm of PROPOSAL which is described in section 2.1.2.

To calculate the total stochastic cross section σ_{stoch} for annihilation, the differential cross section (4.18) is integrated over the entire kinematic range of ϵ . Since $v = 1$, the energy transfer doesn't need to be calculated here. Instead, ϵ needs to be sampled by solving the integral equation

$$\frac{1}{\sigma_{\text{stoch}}} \int_{\epsilon_{\min}}^{\epsilon} \frac{d\sigma}{d\epsilon} d\epsilon = \xi_1 \quad (4.23)$$

for ϵ with a random number $\xi_1 \in [0, 1]$. With the sampled ϵ , the energies of the created photons are set to

$$E_{\gamma,1} = (E + m)\epsilon, \quad E_{\gamma,2} = (E + m)(1 - \epsilon). \quad (4.24)$$

Furthermore, the photons inherit the direction of the initial positron with an additional deflection of a polar angle θ according to (4.20) and (4.21) as well as an azimuth angle Φ sampled via

$$\Phi_{\gamma,1} = 2\pi\xi_2, \quad \Phi_{\gamma,2} = (2\pi\xi_2 + \pi) \bmod 2\pi, \quad (4.25)$$

where $\xi_2 \in [0, 1]$ is an additional random number. After an annihilation interaction, PROPOSAL returns the created photons and stops the particle propagation.

Figure 4.6 shows an energy spectrum of secondary particles produced by positrons where annihilation is enabled. Since annihilation interactions are always stochastic with $v = 1$, the process is not influenced by the energy cut settings, resulting in stochastic losses with $E \cdot v < e_{\text{cut}}$. Quantitatively, the annihilation interaction is, as well as the other processes, suppressed compared to bremsstrahlung processes. However, for energy losses around 1 GeV, a contribution to the secondary spectrum at a level of a few percents can be observed.

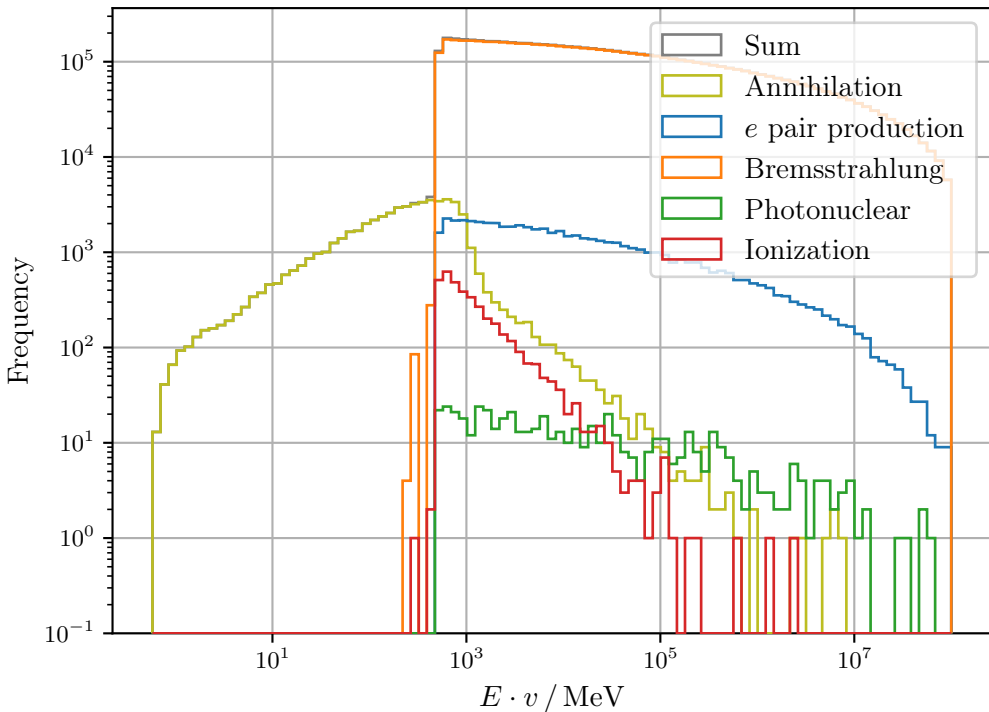


Figure 4.6: Secondary particle energy spectrum for 10^5 positrons with an initial energy of 10^8 MeV, propagated in air. Electron-positron annihilation is enabled. The histogram shows the frequency of the stochastic losses during propagation, classified by the type of energy loss. The energy cut applied here is $e_{\text{cut}} = 500$ MeV. Note that the annihilation process is not affected by the cut settings since the relative energy transfer v is always 1.

4.2 Photon propagation in PROPOSAL

Since photons are massless and uncharged, their interactions differ strongly from interactions of electrons, muons and tauons. Possible photon interactions are the production of electron-positron pairs, Compton scattering and the photoelectric effect. While the implementation of the first two processes is described in the following sections, the photoelectric effect is neglected since its relevance is limited to energies $E \ll 2m_e$. However, photons with energies below $2m_e$ are irrelevant for the further development of an electromagnetic shower due to their inability to produce secondary particles.

4.2.1 Pair production by photons

Photo pair production, called electron-positron pair production in the further course of this section (although not to be confused with the creation of an electron-positron pair by an ingoing lepton), describes the creation of an electron-positron pair by an ingoing photon in the field of an atomic nucleus. A Feynman diagram for the process is shown in figure 4.7. Electron-positron pair production is the dominant

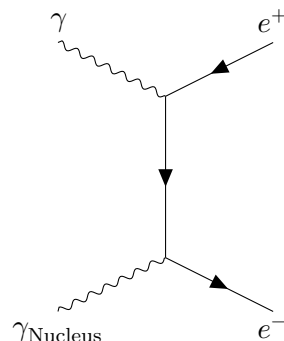


Figure 4.7: Feynman diagram in leading order for electron-positron pair production by an ingoing photon near a nucleus. The nucleus is necessary to conserve energy and momentum during the interaction.

interaction of photons in matter for energies above several MeV and is therefore essential for the propagation of high energy photons.

Theoretical description

The process of electron-positron pair production is described by quantum electrodynamics and a differential cross section exact to order α^3 is provided by [45]. However, the evaluation of this expression is too complicated for a direct implementation. Based on [45, Eq. 3.9], an approximated expression is given by

$$\frac{d\sigma}{dx} = \frac{\alpha r_e^2 x E_\gamma}{p} \left\{ \left(\frac{4}{3}x^2 - \frac{4}{3}x + 1 \right) \times \left[Z^2 \left(\varphi_1 - \frac{4}{3} \ln(Z) - 4f(z) \right) + Z \left(\psi_1 - \frac{8}{3} \ln(Z) \right) \right] - \frac{2}{3}x(1-x) \left[Z^2 (\varphi_1 - \varphi_2) + Z(\psi_1 - \psi_2) \right] \right\} \quad (4.26)$$

with $x = E_-/E_\gamma$ where E_γ is the energy of the initial photon, E_- the energy of the produced electron and p its absolute momentum. The function $f(z)$ describes the Coulomb correction and is defined as

$$f(z) = 1.202z - 1.0369z^2 + 1.008 \frac{z^3}{1+z}, \quad z = \left(\frac{Z}{137} \right)^2. \quad (4.27)$$

While the approximate differential cross section ignores effects from nuclear form factors, which are only important for large production angles, the effects from the atomic form factors are described by the functions φ_1, φ_2 (elastic scattering part) and ψ_1, ψ_2 (inelastic scattering part). The description used for the atomic form factors varies with Z , the resulting expressions for φ and ψ are given in appendix A.

Since the photon must provide the rest mass of both the electron and the positron, the kinematic limits of the process are given by

$$E \geq 2m_e, \quad x_{\min} = \frac{m_e}{E_\gamma}, \quad x_{\max} = 1 - \frac{m_e}{E_\gamma}. \quad (4.28)$$

For high energies, the angles between the photon and the produced leptons are very small and its directions are dominated by multiple scattering effects rather than the initial production angles. Therefore, it is sufficient to treat the calculation of the angular distribution of the electrons and positrons approximately. An approximative double differential cross section describing the angular distribution based on [45, Eq. 3.5] is given by

$$\begin{aligned} \frac{d^2\sigma}{d\theta dp} &= \frac{2\alpha^3 E_-^2}{\pi E_\gamma m_e^4} \sin(\theta) \left[\left(\frac{2x(1-x)}{(1+l)^2} - \frac{12lx(1-x)}{(1+l)^4} \right) G_2(\infty) \right. \\ &\quad \left. + \left(\frac{2x^2 - 2x + 1}{(1+l)^2} + \frac{4lx(1-x)}{(1+l)^4} \right) (X - 2Z^2 f(z)) \right] \end{aligned} \quad (4.29)$$

with

$$l = \frac{E_-^2 \theta^2}{m_e^2}, \quad G_2(\infty) = Z^2 + Z,$$

and the angle θ between the initial photon and the produced electron. The function X , describing the influence of atomic form factors, varies with Z and is defined in appendix A.

Implementation in PROPOSAL

The electron-positron pair production process for photons described in the previous section can be enabled in PROPOSAL by setting the keyword `photopair` in the configuration file to `PhotoPairTsai`.

Since the initial photon ceases to exist after the interaction and transfers its whole energy to the created electron-positron pair, the process is always stochastic with a relative energy transfer of $v = 1$. This requires, very similar to the annihilation process, which is the reverse process of pair production (see 4.1.3 for a description), adjustments to the propagation algorithm of PROPOSAL.

To obtain the total stochastic cross section σ_{stoch} for electron-positron pair production, the differential cross section 4.26 is integrated over the entire kinematic range of x . While the relative energy transfer $v = 1$ is already known, the parameter x , describing the asymmetry of the energy transfer, needs to be sampled by solving the integral equation

$$\frac{1}{\sigma_{\text{stoch}}} \int_{x_{\min}}^x \frac{d\sigma}{dx} dx = \xi_1 \quad (4.30)$$

for x with a random number $\xi_1 \in [0, 1]$. The energy of the electron E_- , respectively the energy of the positron E_+ , is set to

$$E_- = x E_\gamma, \quad E_+ = (1 - x) E_\gamma. \quad (4.31)$$

To offer different levels of accuracy in the simulation of the angular distribution, two options are available to describe the angles between the initial photon and the created electron and positron. Firstly, the double-differential cross section (4.29) can be used to sample the polar angle θ for both the electron and the positron by solving, once for each particle, the integral equation

$$\left(\frac{d\sigma}{dp}(p^*) \right)^{-1} \int_0^\theta \frac{d^2\sigma}{d\theta dp}(p^*) d\theta = \xi_2 \quad (4.32)$$

for θ where $\xi_2 \in [0, 1]$ is an additional random number and $p = p^*$ the fixed absolute momentum of the electron, respectively the positron. Alternatively, a simpler method suggested by [24] can be applied where the angle of both particles is set to

$$\theta = \frac{m_e}{E_\gamma}. \quad (4.33)$$

For both methods, the azimuth angle Φ is sampled via

$$\Phi_- = 2\pi\xi_3, \quad \Phi_+ = (2\pi\xi_3 + \pi) \bmod 2\pi, \quad (4.34)$$

where $\xi_3 \in [0, 1]$ is an additional random number.

Figure 4.8 shows a comparison of the two available sampling methods. For high energies as well as for analyses where the exact distribution of θ is irrelevant, the simple expression according to (4.33) provides an adequate description of the production angle.

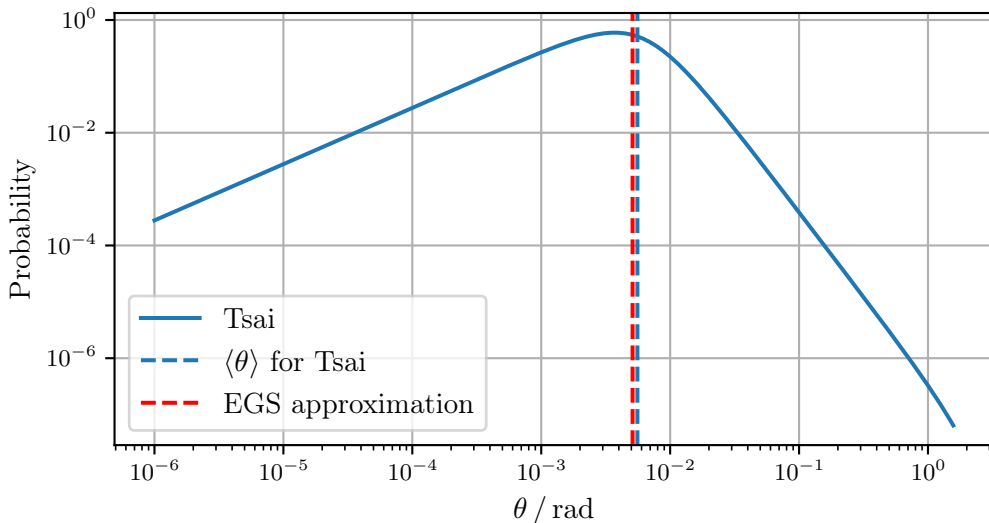


Figure 4.8: Distribution of pair production angles in air with an initial particle energy of $E_\gamma = 10^2$ eV. The vertical line labeled "EGS approximation" shows the production angle according to (4.33), the line labeled "Tsai" shows the distribution for the production angle according to (4.32) where $\langle \theta \rangle$ denotes the mean of this distribution. For this plot, $x = 0.85$ has been used. Note that the distribution of Tsai is affected by the choice of x , however, the expression according to EGS is independent of x .

To use the calculation of the production angles according to (4.32), the keyword `photoangle` in the configuration file can be set to `PhotoAngleTsaiIntegral`, to

use the method from (4.33), the keyword can be set to `PhotoAngleEGS`. Per default, both particles inherit the direction of the initial photon, i.e. the production angle is neglected. This behavior can be enabled explicitly by setting the keyword to `PhotoAngleNoDeflection`.

4.2.2 Compton scattering

Compton scattering describes the scattering of a photon by a charged particle, here an atomic electron, causing a deflection of the initial photon and a reduction of its energy. A Feynman diagram for the interaction is shown in figure 4.9. For photons with an energy between several 100 keV and several 10 MeV, Compton scattering is the dominant interaction process.

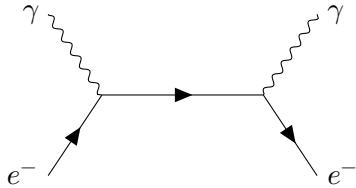


Figure 4.9: Feynman diagram in leading order for Compton scattering. The diagram shown here represents the s -channel contribution.

Theoretical description

Under the assumption that the binding energy of the atomic electrons can be neglected, which is an adequate approximation especially for photon energies that are high enough to be relevant for shower propagation, i.e. $E > 2m_e$, the differential cross section for Compton scattering is given by the Klein-Nishina formula [31]. Based on the formulation of the Klein-Nishina formula in [24], the differential cross section can be written as

$$\frac{d\sigma}{dv} = \frac{Z\pi r_e^2 m_e}{E} \left(\frac{C_1}{\varepsilon^2} + \frac{C_2}{\varepsilon} + C_3 + \varepsilon \right) \quad (4.35)$$

with

$$\varepsilon = 1 - v, \quad C_1 = \frac{m_e^2}{E^2}, \quad (4.36)$$

$$C_2 = 1 - 2C_1 \left(1 + \frac{E}{m_e} \right), \quad C_3 = C_1 \left(1 + 2 \frac{E}{m_e} \right). \quad (4.37)$$

To obtain a relation between θ , the angle between the initial photon and the scattered photon, and the involved energies, using (4.19) with

$$\begin{aligned} E_1 &= E, & m_1 = m_3 &= 0, \\ E_2 &= m_e, & m_2 = m_4 &= m_e, \\ E_3 &= (1 - v)E := E', \end{aligned}$$

according to the kinematics for Compton scattering, yields

$$\cos(\theta) = 1 - \left(\frac{m_e}{E'} - \frac{m_e}{E} \right). \quad (4.38)$$

By solving (4.38) for E' , the well-known relation

$$E' = \frac{E}{1 + \frac{E}{m_e}(1 - \cos(\theta))} \quad (4.39)$$

can be obtained. Setting $\cos(\theta) = \pm 1$ in (4.38) yields the kinematic limits

$$v_{\min} = 0, \quad v_{\max} = \frac{1}{\frac{m_e}{2E} + 1}, \quad (4.40)$$

for Compton scattering.

Implementation in PROPOSAL

Compton scattering, as described in the previous section, can be enabled in PROPOSAL by setting the keyword `compton` in the configuration file to `ComptonKleinNishina`.

Figure 4.10 shows the Klein-Nishina formula for several energies. While the differential cross section is evenly distributed for small energies, a peak towards the forward direction can be seen for higher energies.

To evaluate the integrals (2.6), (2.17) and (2.18) numerically for Compton scattering calculations, the substitution $t = \ln(1 - v)$ is used to avoid occurring numerical problems for $v \rightarrow 1$ at high energies.

In a stochastic Compton interaction, the initial photon is deflected by a polar angle θ according to (4.38) while the azimuth Φ is selected randomly in the range $[0, 2\pi]$.

The total cross section for Compton scattering, compared to the total cross section for electron-positron pair production by photons, is shown in figure 4.11. As expected, electron-positron pair production is the dominant photon interaction in matter for high energies with a transition to Compton scattering as the dominant process at an energy below about 20 MeV.

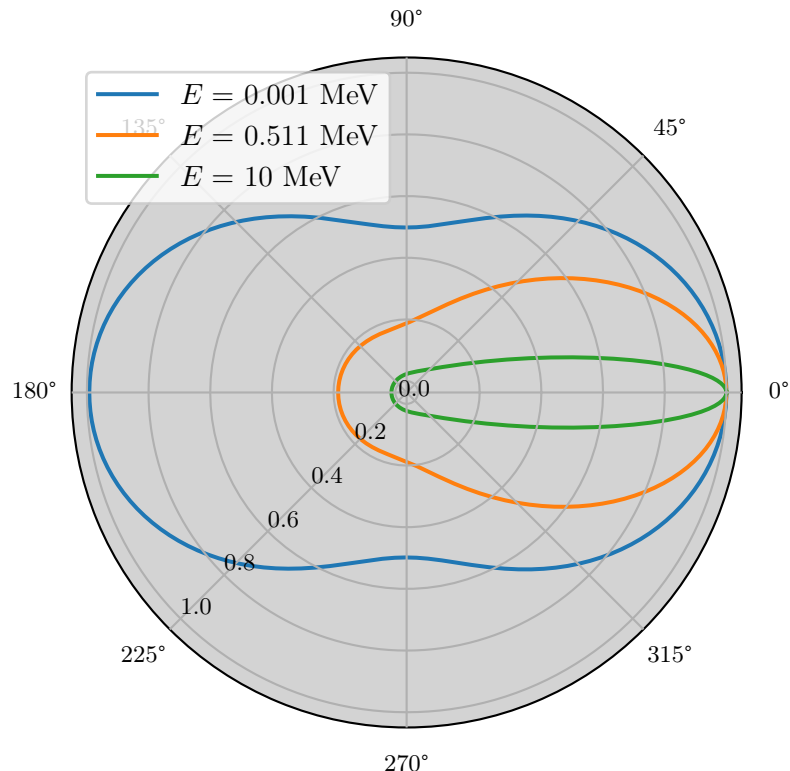


Figure 4.10: Plot showing the differential Compton Scattering cross section in $\cos(\theta)$ for different photon energies according to the Klein-Nishina formula. The angular coordinate determines the deflection angle of the initial photon, the radial axis describes the differential cross section in arbitrary units.

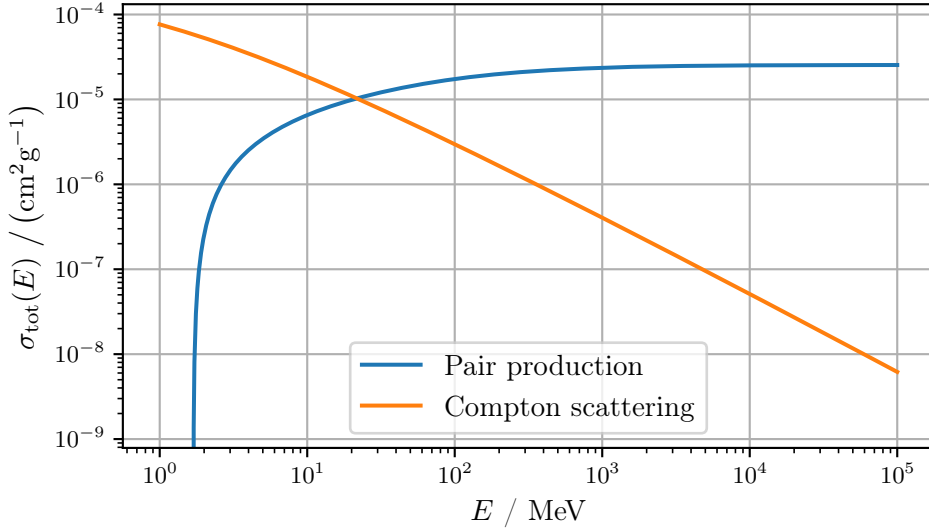


Figure 4.11: Total cross section of Compton scattering in comparison to the total cross sections of electron positron pair production for photons in air. The total cross section is obtained by setting $e_{\text{cut}} \approx 0$.

4.3 Electromagnetic shower propagation with PROPOSAL

With the improvement of electron and positron propagation, as described in section 4.1, as well as the implementation of photon propagation, as described in section 4.2, PROPOSAL can be used to simulate all particles in an electromagnetic shower. As a proof of concept, the simulation of a simple electromagnetic shower with PROPOSAL as a model for electromagnetic interactions is presented.

```

particle list = [primary particle]
shower data = []
while particle list not empty do
    extract first element from particle list
    propagate extracted particle
    save information on particle track in shower data
    append all produced secondary particles to particle list
end
```

Algorithm 1: Simplified shower propagation algorithm.

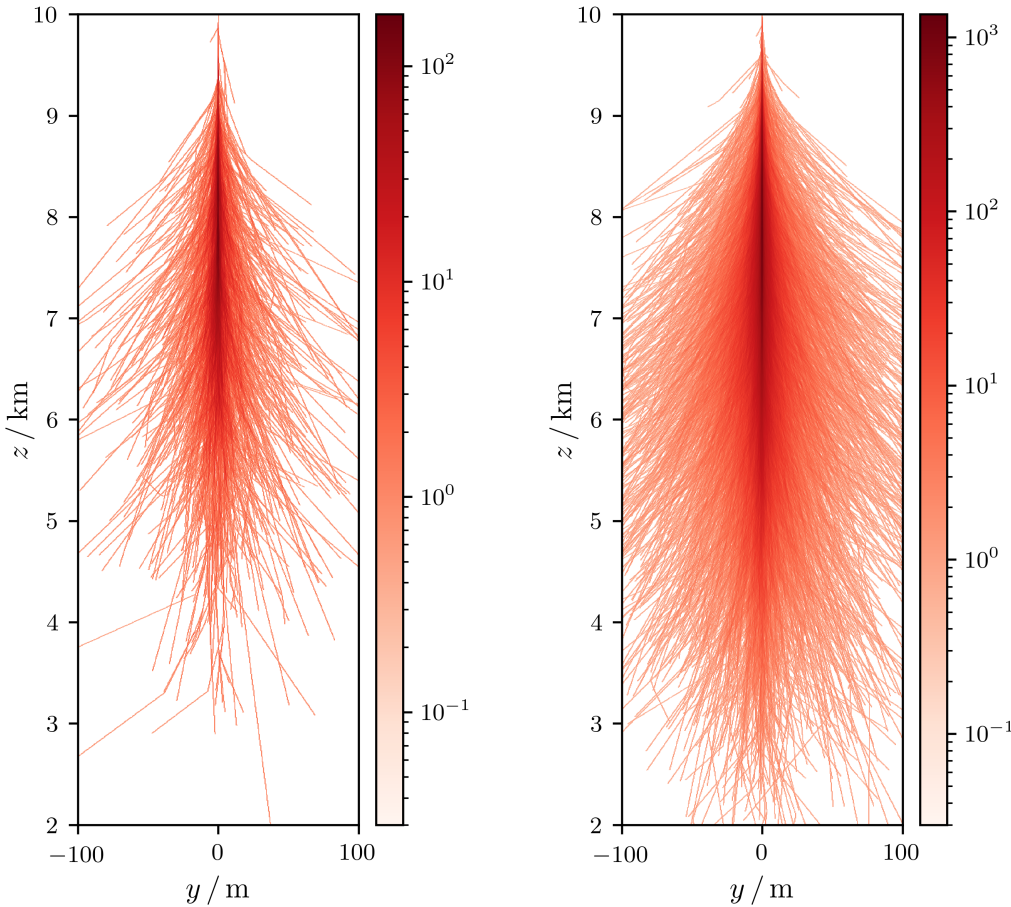
The basic algorithm used for the simulation of an electromagnetic shower is shown in algorithm 1. While the general algorithm is implemented using a Python script, the step "propagate extracted particle" is conducted by PROPOSAL. It can be

seen that the structure of the algorithm corresponds to a breadth-first search since particles that were first added to the list are also propagated first (**First In, First Out** principle).

For each stochastic interaction, the position of the stochastic interaction, the type of the particle causing the stochastic interaction, the energy of the initial particle before the stochastic interaction as well as the position of the previous stochastic interaction are saved in the shower data list. This information can be used to reconstruct the shower development. In the last step, electrons and positrons from pair production by photons, photons from electron-positron annihilation as well as bremsstrahlung photons created by electrons or positrons are taken from the PROPOSAL output and added to the particle list. Other particles such as electrons and positrons from pair production by other leptons are neglected in this version of the algorithm.

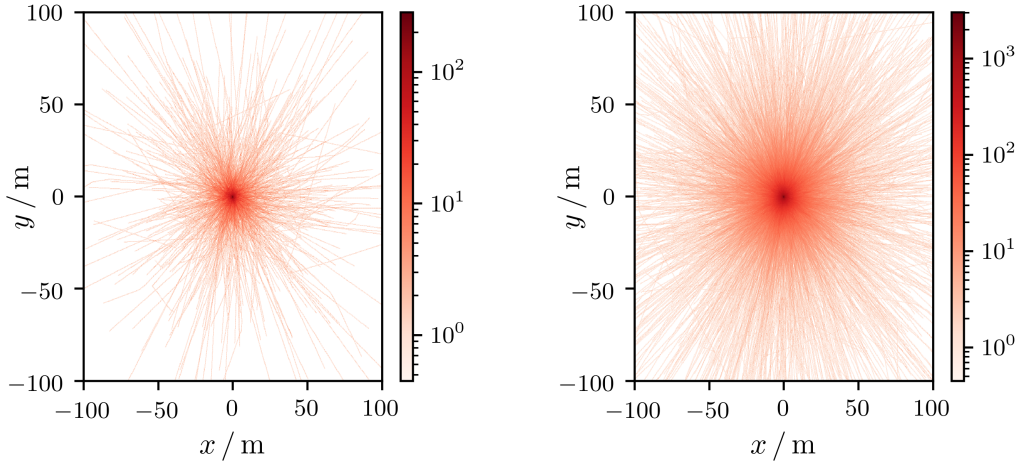
The atmosphere for the simulated showers is described by homogeneous air with a density of $\rho = 1.205 \text{ kg/cm}^3$ corresponding to the properties of air at sea level. Therefore, the variation of the density with altitude is not taken into account. The primary particle for the electromagnetic shower is a photon initialized at a height of $z = 10 \text{ km}$ directed towards the ground at $z = 0 \text{ km}$ which is described as standard rock. The cut settings for the propagation of all particles are set to $e_{\text{cut}} = 50 \text{ MeV}$ with no v_{cut} .

Figures 4.12 and 4.13 show the track densities of two electromagnetic showers with different initial photon energies. The plots are obtained by connecting the positions of two consecutive stochastic losses of a particle and plotting the resulting tracks in a high-resolution histogram. Both the projection onto the zy -plane in figure 4.12 and the projection onto the xy -plane in figure 4.13 show that the showers consist of a core with a very high particle density that decreases with distance from the initial shower axis. In figure 4.14 and figure 4.15, the shower profiles for both showers, i.e. the number of particles in the xy -plane as a function of the distance z from the ground, are shown.



(a) Shower for an initial photon energy of 10^6 MeV. (b) Shower for an initial photon energy of 10^7 MeV.

Figure 4.12: Two electromagnetic showers induced by a photon at $z = 10$ km. The color bar describes the particle density (electrons, positrons and photons combined) in approximate counts. Only particle tracks with an energy above 50 MeV at the end of the track are shown. The shower has been projected onto the zy -plane in the laboratory frame.



(a) Shower for an initial photon energy of 10^6 MeV. (b) Shower for an initial photon energy of 10^7 MeV.

Figure 4.13: Two electromagnetic showers induced by a photon at $z = 10$ km. The color bar describes the particle density (electrons, positrons and photons combined) in approximate counts. Only particle tracks with an energy above 50 MeV at the end of the track are shown. The shower has been projected onto the xy -plane in the laboratory frame.

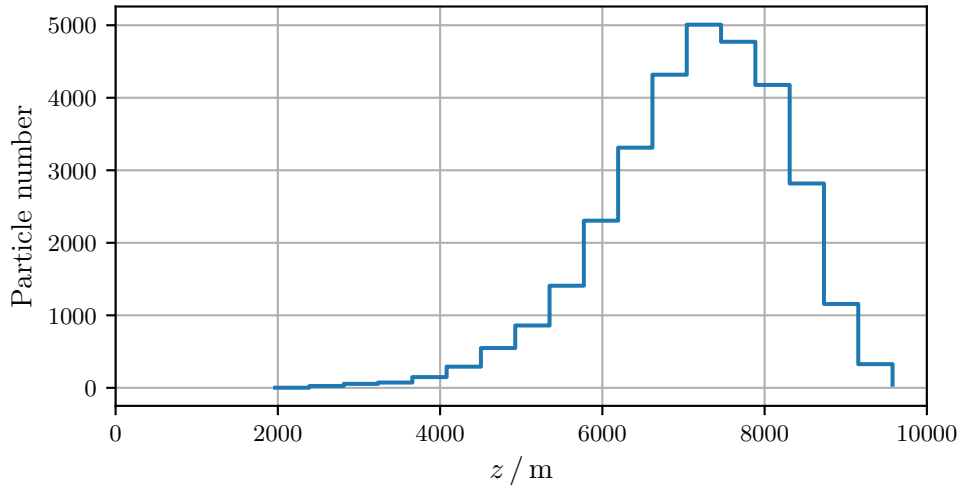


Figure 4.14: Shower profile of the electromagnetic shower with an initial photon energy of 10^6 MeV.

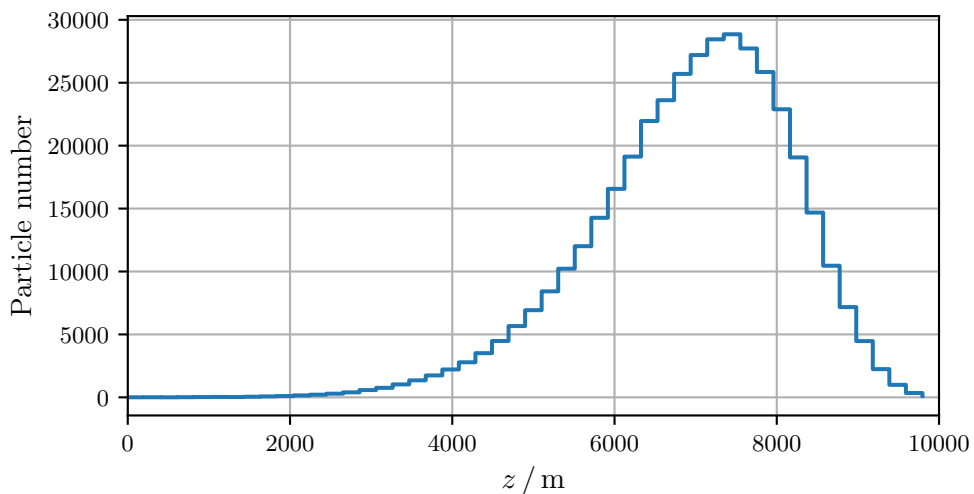


Figure 4.15: Shower profile of the electromagnetic shower with an initial photon energy of 10^7 MeV.

5 Conclusion and outlook

5.1 Conclusion

In this thesis, two rare processes, the production of muon pairs and the weak interaction of charged leptons, have been implemented as new interactions in PROPOSAL. While it has been shown that their contribution to the overall energy loss of muons is negligible, it is necessary to conduct further, explicit analyses to investigate the significance of their produced signatures. The current status of PROPOSAL offers an appropriate framework for this task.

With the implementation of the Berger-Seltzer formula as a correct parametrization of electron ionization losses as well as the implementation of an optimized bremsstrahlung parametrization, the description of electron propagation in PROPOSAL has been improved. To be able to provide all interactions necessary to accurately describe the propagation of positrons as well, annihilation has been added as an additional process. Furthermore, the propagation of photons with PROPOSAL is now possible due to the implementation of electron-positron pair production and Compton scattering as new, photon-specific processes. This extension portrays a new application possibility of PROPOSAL since before, PROPOSAL exclusively supported the propagation of charged leptons.

Since electron, positron and photon interactions are now described accurately, PROPOSAL can be used as a software to propagate all particles of an electromagnetic shower. As a proof of concept, a simple Python routine, using the particle propagation of PROPOSAL, has been written to simulate electromagnetic showers. Based on this work, it is possible to implement PROPOSAL as an electromagnetic model used by CORSIKA 8, enabling the simulation of a full atmospheric air shower. However, it is necessary to enable particle propagation in inhomogeneous media with PROPOSAL, describing the atmospheric density profile, which is part of an ongoing thesis.

To validate the results of this work, cross-checks with other works are necessary. One important cross-check, possible after the implementation of PROPOSAL in CORSIKA has been completed, is a comparison with the EmCa (**E**lectromagnetic-**C**ascades) simulation package [35] which provides an alternative approach to describe

electromagnetic air showers. Comparing the characteristics of full extensive air showers simulated with CORSIKA 8, longitudinal shower profiles for example, using either PROPOSAL, EmCa or other electromagnetic models such as EGS or Geant4 can give indications about the accuracy of PROPOSAL or provide hints where further improvements can be made.

5.2 Outlook

The aim of this thesis has been the implementation of all processes essential for the propagation of particles in an electromagnetic shower. Therefore, further improvements may be made in future works to provide a more detailed simulation of the shower development. Examples are the implementation of the creation of muon pairs by photons, which is important for muonic air shower components [21], or the deflection of charged particles in the Earth's magnetic field. Furthermore, the deflection of the initial particle in stochastic interactions has only been implemented for Compton scattering. However, the deflection in other processes such as stochastic bremsstrahlung interactions may be of importance for the lateral shower distribution. These deflection effects can, if corresponding theoretical descriptions are available, easily be implemented in PROPOSAL.

As mentioned in section 4.1.1, the implemented Berger-Seltzer formula does, unlike the ionization formula used for muon and tau leptons, not include higher-order corrections. Especially for light media such as air and ice, these corrections from bremsstrahlung at atomic electrons may induce relevant effects. To evaluate these effects numerically, theoretical calculations have to be conducted.

In a past thesis, the possibility to optimize the runtime of PROPOSAL by using graphics processing units (GPUs) has been investigated [18]. Additionally, the parallelized creation and propagation of Cherenkov photons on GPUs in CORSIKA is currently under development [6]. To avoid time-consuming information transfer between the GPU and other hardware components, it would desirable to simulate both the electromagnetic shower component and Cherenkov photons on GPUs. Therefore, both CORSIKA and PROPOSAL may benefit from continuing the work started in [18].

A Atomic form factors for photo pair production

Atomic form factors are necessary to describe the effects on electron-positron pair production by photons due to the field of atomic electrons. These effects are firstly the screening of the nuclear Coulomb field, described by the elastic atomic form factor G_2^{el} , and secondly events where the photon scatters from the electron field screened by the nucleus, described by the inelastic atomic form factor G_2^{inel} . The contributions from the atomic form factors are only relevant for electron-positron pair production at small production angles which is the usual use case for high energy photon propagation. To obtain the functions φ_i , ψ_i and $X = X_{\text{el}} + X_{\text{inel}}$, which are used to parametrize the information from these atomic form factors, integrations of G_2 over kinematic variables are necessary. The different expressions used for these functions, varying with Z , are presented in the following.

A.1 Hydrogen and Helium

For $Z = 1$, the atomic form factors are known exactly while for $Z = 2$, an approximative model leading to a similar analytic expression can be used. These form factors can be integrated analytically leading to the expressions [45]

$$\begin{aligned} \varphi_1 &= \frac{4}{3} \ln(Z) + 4 \ln\left(\frac{1}{2\eta\alpha}\right) + \frac{13}{3} - 2 \ln(1 + C^2) \\ &\quad - \frac{13}{2} C \arctan(C^{-1}) + \frac{1}{6} \frac{1}{1 - C^{-2}}, \end{aligned} \tag{A.1}$$

$$\begin{aligned} \varphi_2 &= \frac{4}{3} \ln(Z) + 4 \ln\left(\frac{1}{2\eta\alpha}\right) + \frac{11}{3} - 2 \ln(1 + C^2) \\ &\quad + 25C^2(1 - C \arctan(C^{-1})) - 14C^2 \ln(1 + C^{-2}), \end{aligned} \tag{A.2}$$

$$\begin{aligned} \psi_1 &= \frac{8}{3} \ln(Z) + 4 \ln\left(\frac{1}{2\eta\alpha}\right) + \frac{23}{3} - 2 \ln(1 + C^2) \\ &\quad - 17.5C \arctan C^{-1} + 8C^2 \ln(1 + C^{-2}) - \frac{1}{6} \frac{1}{1 + C^{-2}}, \end{aligned} \tag{A.3}$$

$$\begin{aligned}\psi_2 = & \frac{8}{3} \ln(Z) + 4 \ln\left(\frac{1}{2\eta\alpha}\right) + \frac{21}{3} - 2 \ln(1 + C^2) \\ & - 105C^2(1 - C \arctan(C^{-1})) + 50C^2 \ln(1 + C^{-2}) \\ & - 24C^2 \left[-\ln(C^2) \ln(1 + C^{-2}) + \Phi(1 + C^{-2}) - \Phi(1) \right],\end{aligned}\quad (\text{A.4})$$

$$\begin{aligned}X_{\text{el}} = & Z^2 \left[2 \ln\left(\frac{m_e}{\delta}\right) - \ln(1 + B^2) + \frac{1}{6} - \frac{4}{3} \frac{1}{1 + B^2} \right. \\ & \left. + \frac{1}{6} \frac{1}{(1 + B^2)^2} \right],\end{aligned}\quad (\text{A.5})$$

$$\begin{aligned}X_{\text{inel}} = & Z \left[2 \ln\left(\frac{m_e}{\delta}\right) - \ln(1 + B^2) + \frac{11}{6} - 4B^{-2} \ln(1 + B^2) \right. \\ & \left. + \frac{4}{3} \frac{1}{1 + B^2} - \frac{1}{6} \frac{1}{(1 + B^2)^2} \right],\end{aligned}\quad (\text{A.6})$$

with

$$\begin{aligned}\delta = & \frac{m_e^2}{2E_\gamma x(1-x)}, & C = & \frac{\delta}{2\alpha m_e \eta}, & x = & \frac{E_-}{E_\gamma}, \\ t'_{\min} = & \left(\frac{m_e^2(1+l)}{2E_\gamma x(1-x)} \right)^2, & B = & \frac{2\alpha m_e \eta}{\sqrt{t'_{\min}}}, & l = & \frac{E_-^2 \theta^2}{m_e^2},\end{aligned}$$

where E_γ is the energy of the photon, E_- the energy of the produced electron, θ the angle between the photon and the produced electron and η is defined as

$$\eta = \begin{cases} 1 & \text{if } Z = 1, \\ 1.6875 & \text{if } Z = 2, \end{cases}$$

with the dilogarithm function $\Phi(x)$.

A.2 Lithium and Beryllium

For $Z = 3$ and $Z = 4$, the atomic form factors G_2 are only known numerically. Instead of referring to these values, a simpler approximation for the form factors is used. The parameters of this approximation are chosen in such a way that the results for G_2 are exact in the limits of complete screening and no screening. Based on that, the functions φ_i , ψ_i and $X = X_{\text{el}} + X_{\text{inel}}$ are [45]

$$\varphi_1 = 2(1 + \ln(a^2 Z^{2/3} m_e^2)) - 2 \ln(1 + b^2) - 4b \arctan(b^{-1}), \quad (\text{A.7})$$

$$\begin{aligned}\varphi_2 = & 2 \left(\frac{2}{3} + \ln(a^2 Z^{2/3} m_e^2) \right) - 2 \ln(1 + b^2) \\ & + 8b^2 \left[1 - b \arctan(b^{-1}) - 0.75 \ln(1 + b^{-2}) \right],\end{aligned}\tag{A.8}$$

$$\psi_1 = 2 \left(1 + \ln(a'^2 Z^{4/3} m_e^2) \right) - 2 \ln(1 + b'^2) - 4b' \arctan(b^{-1}),\tag{A.9}$$

$$\begin{aligned}\psi_2 = & 2 \left(\frac{2}{3} + \ln(a'^2 Z^{4/3} m_e^2) \right) - 2 \ln(1 + b'^2) \\ & + 8b'^2 \left[1 - b \arctan(b'^{-1}) - 0.75 \ln(1 + b'^{-2}) \right],\end{aligned}\tag{A.10}$$

$$X_{\text{el}} = Z^2 \left[\ln \left(\frac{a^2 m_e^2 (1+l)^2}{a^2 t'_{\min} + 1} \right) - 1 \right],\tag{A.11}$$

$$X_{\text{inel}} = Z \left[\ln \left(\frac{a'^2 m_e^2 (1+l)^2}{a'^2 t'_{\min} + 1} \right) - 1 \right],\tag{A.12}$$

with

$$\begin{aligned}a = & \begin{cases} \frac{100}{m_e} Z^{-1/3} & \text{if } Z = 3, \\ \frac{106}{m_e} Z^{-1/3} & \text{if } Z = 4, \end{cases} \\ a' = & \begin{cases} \frac{418.6}{m_e} Z^{-2/3} & \text{if } Z = 3, \\ \frac{571.4}{m_e} Z^{-2/3} & \text{if } Z = 4, \end{cases}\end{aligned}$$

and $b = a\delta$, $b' = a'\delta$.

A.3 Heavier elements

For $Z > 4$, the Thomas-Fermi model of the atom is used to evaluate the atomic form factors. The parameters in (A.7) to (A.12) were adapted to fit the numerical values obtained from the Thomas-Fermi model, yielding the expressions [45]

$$\begin{aligned}\varphi_1(\gamma) = & 20.863 - 2 \ln(1 + (0.55846\gamma)^2) \\ & - 4 \left[1 - 0.6 \exp(-0.9\gamma) - 0.4 \exp(-1.5\gamma) \right],\end{aligned}\tag{A.13}$$

$$\varphi_2(\gamma) = \varphi_1(\gamma) - \frac{2}{3} \frac{1}{1 + 6.5\gamma + 6\gamma^2},\tag{A.14}$$

$$\begin{aligned}\psi_1(\epsilon) &= 28.34 - 2 \ln(1 + (3.621\epsilon)^2) \\ &\quad - 4 \left[1 - 0.7 \exp(-8\epsilon) - 0.3 \exp(-29.2\epsilon) \right],\end{aligned}\tag{A.15}$$

$$\psi_2(\epsilon) = \psi_1(\epsilon) - \frac{2}{3} \frac{1}{1 + 40\epsilon + 400\epsilon^2},\tag{A.16}$$

$$X_{\text{el}} = Z^2 \left[\ln \left(\frac{a^2 m_e^2 (1+l)^2}{a^2 t'_{\min} + 1} \right) - 1 \right],\tag{A.17}$$

$$X_{\text{inel}} = Z \left[\ln \left(\frac{a'^2 m_e^2 (1+l)^2}{a'^2 t'_{\min} + 1} \right) - 1 \right],\tag{A.18}$$

with

$$\gamma = \frac{200\delta}{m_e Z^{1/3}}, \quad \epsilon = \frac{200\delta}{m_e Z^{2/3}}, \quad a = 111.7 \frac{Z^{-1/3}}{m_e}, \quad a' = 724.2 \frac{Z^{-2/3}}{m_e}.$$

B Constants and variables

The variables listed in table B.1 are used for this thesis as well as in PROPOSAL, the corresponding numerical values are obtained from [44].

Table B.1: Definitions and numerical values of constants and variables.

Variable	Definition	Numerical value
α	Fine-structure constant	0.007 297 352 566 4
N_A	Avogadro Constant	$6.022\,140\,857 \cdot 10^{23}$ /mol
m_e	Electron mass	0.510 998 946 1 MeV
m_μ	Muon mass	105.658 374 5 MeV
r_e	Classical electron radius	$2.817\,940\,322\,7 \cdot 10^{-13}$ cm
r_μ	Classical muon radius	$r_e \cdot m_e \cdot m_\mu^{-1}$
Z	Atomic number	
A	Atomic mass number	
e	Euler's number	2.718 281 828 459 045
π		3.141592653589793

C Reproducibility

To create the figures presented in this thesis, the programming language *Python 3.8.1*, together with the Python packages *matplotlib v3.1.2* [25], *NumPy v1.18.0* [38] as well as *SciPy 1.4.1* [46], has been used. Feynman diagrams have been produced using the TikZ-Feynman L^AT_EX-package [16]. The PROPOSAL version used to produce all results has been tagged and is publicly available on GitHub under the link <https://github.com/Jean1995/PROPOSAL/releases/tag/thesis>.

All results from this thesis may be reproduced using the scripts available on GitHub under the link <https://github.com/Jean1995/Masterarbeit>, this requires installing the corresponding versions of the above-mentioned packages. If *GNU Make* and a L^AT_EX compiler are available, executing the console command `make` reproduces all plots as well as the thesis itself.

Bibliography

- [1] M. G. Aartsen et al. “Search for astrophysical tau neutrinos in three years of IceCube data”. In: *Physical Review D* 93.2 (Jan. 2016). ISSN: 2470-0029. DOI: 10.1103/physrevd.93.022001. arXiv: 1509.06212.
- [2] M. G. Aartsen et al. “The IceCube Neutrino Observatory: instrumentation and online systems”. In: *Journal of Instrumentation* 12.03 (Mar. 2017). ISSN: 1748-0221. DOI: 10.1088/1748-0221/12/03/p03012. arXiv: 1612.05093.
- [3] R. Abbasi et al. “The IceCube data acquisition system: Signal capture, digitization, and timestamping”. In: *Nuclear Instruments and Methods in Physics Research Section A: Accelerators, Spectrometers, Detectors and Associated Equipment* 601.3 (Apr. 2009), pp. 294–316. ISSN: 0168-9002. DOI: 10.1016/j.nima.2009.01.001. arXiv: 0810.4930.
- [4] Halina Abramowicz and Aharon Levy. *The ALLM parameterization of $\sigma_{tot}(\gamma^* p)$ - an update*. 1997. arXiv: hep-ph/9712415 [hep-ph].
- [5] J. Ahrens et al. “Sensitivity of the IceCube detector to astrophysical sources of high energy muon neutrinos”. In: *Astroparticle Physics* 20.5 (Feb. 2004), pp. 507–532. ISSN: 0927-6505. DOI: 10.1016/j.astropartphys.2003.09.003. arXiv: astro-ph/0305196.
- [6] D. Baack. “Performance optimization of air shower simulations with CORSIKA”. In: *36th International Cosmic Ray Conference (ICRC2019)*. Vol. 36. International Cosmic Ray Conference. July 2019, p. 181.
- [7] M. J. Berger et al. “Stopping Powers for Electrons and Positions (ICRU Report No. 37)”. In: *Journal of the International Commission on Radiation Units and Measurements* 2 (Apr. 1984). ISSN: 1473-6691. DOI: 10.1093/jicru/os19.2. Report37.
- [8] H. A. Bethe and J. Ashkin. “Passage of radiations through matter”. In: *Experimental Nuclear Physics* 1 (1953), p. 253.
- [9] A. Butkevich and S. Mikheyev. “Cross section of the muon-nuclear inelastic interaction”. In: *Journal of Experimental and Theoretical Physics* 95 (Sept. 2001). DOI: 10.1134/1.1499897. arXiv: hep-ph/0109060.
- [10] Dmitry Chirkin and Wolfgang Rhode. *Propagating leptons through matter with Muon Monte Carlo (MMC)*. 2004. arXiv: hep-ph/0407075 [hep-ph].

- [11] Amanda Cooper-Sarkar. “Proton Structure from HERA to LHC”. In: *40th International Symposium on Multiparticle Dynamics (ISMD 2010)*. 2010. arXiv: 1012.1438 [hep-ph].
- [12] Amanda Cooper-Sarkar, Philipp Mertsch and Subir Sarkar. “The high energy neutrino cross-section in the Standard Model and its uncertainty”. In: *Journal of High Energy Physics* 2011.8 (Aug. 2011). ISSN: 1029-8479. DOI: 10.1007/jhep08(2011)042. arXiv: 1106.3723.
- [13] D. F. Cowen. “Tau Neutrinos in IceCube”. In: *Journal of Physics: Conference Series* 60 (Mar. 2007), pp. 227–230. DOI: 10.1088/1742-6596/60/1/048.
- [14] Simon Duane, Alex Bielajew and David W. O. Rogers. *Use of ICRU-37/NBS collision stopping powers in the EGS4 system*. Tech. rep. PIRS-0173. National Research Council Canada, 1989. URL: <https://people.physics.carleton.ca/~drogers/pubs/papers/pirs173.pdf>.
- [15] Mario Dunsch et al. “Recent improvements for the lepton propagator PROPOSAL”. In: *Computer Physics Communications* 242 (Sept. 2019), pp. 132–144. ISSN: 0010-4655. DOI: 10.1016/j.cpc.2019.03.021. arXiv: 1809.07740.
- [16] Joshua P. Ellis. “TikZ-Feynman: Feynman diagrams with TikZ”. In: *Computer Physics Communications* 210 (Feb. 2017), pp. 103–123. ISSN: 0010-4655. DOI: 10.1016/j.cpc.2016.08.019.
- [17] Tomasz Fuchs. “Charmante Myonen im Eis”. PhD thesis. Jan. 2016. DOI: 10.17877/DE290R-17241.
- [18] Tomasz Fuchs. “Leptonpropagation mit PROPOSAL unter Verwendung von Grafikprozessoren”. Master thesis. Technische Universität Dortmund, 2012.
- [19] Malte Geisel-Brinck. “Revision of the multiple scattering algorithms in PROPOSAL”. Bachelor thesis. Technische Universität Dortmund, 2013.
- [20] David J Griffiths. *Introduction to elementary particles; 2nd rev. version*. Physics textbook. New York, NY: Wiley, 2008. ISBN: 9783527406012.
- [21] D. Heck et al. “CORSIKA: A Monte Carlo code to simulate extensive air showers”. In: *Wissenschaftliche Berichte / Forschungszentrum Karlsruhe, Technik und Umwelt* 6019 (1998). URL: https://web.ikp.kit.edu/corsika/physics_description/corsika_phys.pdf.
- [22] Dieter Heck and Tanguy Pierog. *Extensive Air Shower Simulation with CORSIKA: A User’s Guide*. Tech. rep. Karlsruher Institut für Technologie (KIT), Dec. 2019. URL: <https://web.ikp.kit.edu/corsika/usersguide/usersguide.pdf>.
- [23] W. Heitler. *The Quantum Theory of Radiation*. Dover Books on Physics and Chemistry. Dover Publications, 1954. ISBN: 9780486645582.

Bibliography

- [24] Hideo Hirayama et al. *The EGS5 code system*. Tech. rep. Stanford Linear Accelerator Center (SLAC), Dec. 2005. doi: 10.2172/877459.
- [25] J. D. Hunter. “Matplotlib: A 2D graphics environment”. In: *Computing in Science & Engineering* 9.3 (2007), pp. 90–95. doi: 10.1109/MCSE.2007.55.
- [26] I. Kawrakow et al. *The EGSnrc code system: Monte Carlo simulation of electron and photon transport*. Tech. rep. PIRS-701. National Research Council Canada, 2017. URL: <http://nrc-cnrc.github.io/EGSnrc/doc/pirs701-egsnrc.pdf>.
- [27] S. R. Kelner. “Pair production in collisions between muons and atomic electrons”. In: *Physics of Atomic Nuclei* 61.3 (Mar. 1998), pp. 448–456. doi: 10.1134/1855093.
- [28] S. R. Kelner, R. P. Kokoulin and A. A. Petrukhin. “About Cross-section for High-energy Muon Bremsstrahlung”. In: *Preprint of Moscow Engineering Physics Institute* (Jan. 1995).
- [29] S. R. Kelner, R. P. Kokoulin and A. A. Petrukhin. “Direct production of muon pairs by high-energy muons”. In: *Physics of Atomic Nuclei* 63.9 (Sept. 2000), pp. 1603–1611. ISSN: 1562-692X. doi: 10.1134/1.1312894.
- [30] Semyon Khokhlov. “Reconstruction of the spectrum of cascades generated by VHE muons in the IceCube”. In: *Journal of Physics: Conference Series* 1390.1 (2019), p. 012059. doi: 10.1088/1742-6596/1390/1/012059.
- [31] O. Klein and T. Nishina. “Über die Streuung von Strahlung durch freie Elektronen nach der neuen relativistischen Quantendynamik von Dirac”. In: *Zeitschrift fur Physik* 52.11-12 (Nov. 1929), pp. 853–868. doi: 10.1007/BF01366453.
- [32] Jan-Hendrik Köhne. “Der Leptonpropagator PROPOSAL”. PhD thesis. Technische Universität Dortmund, 2013. doi: 10.17877/DE290R-13191.
- [33] R. P. Kokoulin and A. A. Petrukhin. “Influence of the nuclear formfactor on the cross section of electron pair production by high-energy muons”. In: *12th International Conference on Cosmic Rays* 6 (Jan. 1971), pp. 2436–2445.
- [34] V.A. Kudryavtsev, E.V. Korolkova and N.J.C. Spooner. “Narrow muon bundles from muon pair production in rock”. In: *Physics Letters B* 471.2-3 (Dec. 1999), pp. 251–256. ISSN: 0370-2693. doi: 10.1016/s0370-2693(99)01378-7. arXiv: hep-ph/9911493.
- [35] Stephan Meighen-Berger, Anatoli Fedynitch and Matthias Huber. *EmCa – Electromagnetic-Cascades Simulation Package*. 2019. arXiv: 1907.06924.
- [36] W. R. Nelson, H. Hirayama and D. W. O. Rogers. *EGS4 code system*. Tech. rep. Stanford Linear Accelerator Center, Menlo Park, CA (USA), Dec. 1985.

- [37] S. Ohm, C. van Eldik and K. Egberts. “Gamma-Hadron Separation in Very-High-Energy gamma-ray astronomy using a multivariate analysis method”. In: *Astroparticle Physics* 31.5 (June 2009), pp. 383–391. ISSN: 0927-6505. DOI: 10.1016/j.astropartphys.2009.04.001. arXiv: 0904.1136.
- [38] Travis E Oliphant. *A guide to NumPy*. Vol. 1. Trelgol Publishing USA, 2006.
- [39] Maximilian Reininghaus and Ralf Ulrich. “CORSIKA 8 – Towards a modern framework for the simulation of extensive air showers”. In: *EPJ Web of Conferences* 210 (Jan. 2019), p. 02011. DOI: 10.1051/epjconf/201921002011. arXiv: 1902.02822.
- [40] F. Rohrlich and B. C. Carlson. “Positron-Electron Differences in Energy Loss and Multiple Scattering”. In: *Physical Review* 93 (1 Jan. 1954), pp. 38–44. DOI: 10.1103/PhysRev.93.38.
- [41] Bruno Benedetto Rossi. *High-energy particles*. Prentice-Hall physics. New York, NY: Prentice-Hall, 1952. URL: <https://cds.cern.ch/record/99081>.
- [42] Alexander Sandrock. “Higher-order corrections to the energy loss cross sections of high-energy muons”. PhD thesis. Technische Universität Dortmund, 2018. DOI: 10.17877/DE290R-19810.
- [43] Jan Soedingrekso, Alexander Sandrock and Wolfgang Rhode. “The effect of improved high-energy muon cross-sections”. In: *36th International Cosmic Ray Conference (ICRC2019)*. 2019. arXiv: 1910.07050 [hep-ph].
- [44] M. Tanabashi et al. “Review of Particle Physics”. In: *Physical Review D* 98 (3 Aug. 2018), p. 030001. DOI: 10.1103/PhysRevD.98.030001.
- [45] Yung-Su Tsai. “Pair production and bremsstrahlung of charged leptons”. In: *Reviews of Modern Physics* 46 (4 Oct. 1974), pp. 815–851. DOI: 10.1103/RevModPhys.46.815.
- [46] Pauli Virtanen et al. “SciPy 1.0: Fundamental Algorithms for Scientific Computing in Python”. In: *Nature Methods* (2020). DOI: 10.1038/s41592-019-0686-2.

**Eidesstattliche Versicherung
(Affidavit)**

Alameddine, Jean-Marco

Name, Vorname
(Last name, first name)

180483

Matrikelnr.
(Enrollment number)

Ich versichere hiermit an Eides statt, dass ich die vorliegende Bachelorarbeit/Masterarbeit* mit dem folgenden Titel selbstständig und ohne unzulässige fremde Hilfe erbracht habe. Ich habe keine anderen als die angegebenen Quellen und Hilfsmittel benutzt sowie wörtliche und sinngemäße Zitate kenntlich gemacht. Die Arbeit hat in gleicher oder ähnlicher Form noch keiner Prüfungsbehörde vorgelegen.

I declare in lieu of oath that I have completed the present Bachelor's/Master's* thesis with the following title independently and without any unauthorized assistance. I have not used any other sources or aids than the ones listed and have documented quotations and paraphrases as such. The thesis in its current or similar version has not been submitted to an auditing institution.

Titel der Bachelor-/Masterarbeit*:
(Title of the Bachelor's/ Master's* thesis):

Simulation of rare processes and electromagnetic shower components
within the Monte Carlo propagation library PROPOSAL

*Nichtzutreffendes bitte streichen
(Please choose the appropriate)

Iserlohn, 14.2.2020

Ort, Datum
(Place, date)

J. Alameddine

Unterschrift
(Signature)

Belehrung:

Wer vorsätzlich gegen eine die Täuschung über Prüfungsleistungen betreffende Regelung einer Hochschulprüfungsordnung verstößt, handelt ordnungswidrig. Die Ordnungswidrigkeit kann mit einer Geldbuße von bis zu 50.000,00 € geahndet werden. Zuständige Verwaltungsbehörde für die Verfolgung und Ahndung von Ordnungswidrigkeiten ist der Kanzler/die Kanzlerin der Technischen Universität Dortmund. Im Falle eines mehrfachen oder sonstigen schwerwiegenden Täuschungsversuches kann der Prüfling zudem exmatrikuliert werden. (§ 63 Abs. 5 Hochschulgesetz - HG -).

Die Abgabe einer falschen Versicherung an Eides statt wird mit Freiheitsstrafe bis zu 3 Jahren oder mit Geldstrafe bestraft.

Die Technische Universität Dortmund wird gfls. elektronische Vergleichswerkzeuge (wie z.B. die Software „turnitin“) zur Überprüfung von Ordnungswidrigkeiten in Prüfungsverfahren nutzen.

Die oben stehende Belehrung habe ich zur Kenntnis genommen:

Official notification:

Any person who intentionally breaches any regulation of university examination regulations relating to deception in examination performance is acting improperly. This offense can be punished with a fine of up to €50,000.00. The competent administrative authority for the pursuit and prosecution of offenses of this type is the chancellor of TU Dortmund University. In the case of multiple or other serious attempts at deception, the examinee can also be unenrolled, section 63, subsection 5 of the North Rhine-Westphalia Higher Education Act (Hochschulgesetz).

The submission of a false affidavit will be punished with a prison sentence of up to three years or a fine.

As may be necessary, TU Dortmund will make use of electronic plagiarism-prevention tools (e.g. the "turnitin" service) in order to monitor violations during the examination procedures.

I have taken note of the above official notification:**

Iserlohn, 14.2.2020

Ort, Datum
(Place, date)

J. Alameddine

Unterschrift
(Signature)

**Please be aware that solely the German version of the affidavit ("Eidesstattliche Versicherung") for the Bachelor's/ Master's thesis is the official and legally binding version.